MANCHESTER 1824
The University of Manchester

Impaired Mineral Ion Metabolism in a Mouse Model of Targeted Calcium-Sensing Receptor (CaSR) Deletion from Vascular Smooth Muscle Cells

DOI:
10.1681/ASN.2021040585
10.1681/ASN.2021040585

Document Version
Accepted author manuscript

Link to publication record in Manchester Research Explorer

Citation for published version (APA):
Schepelmann, M., Ranieri, M., Lopez-Fernandez, I., Webberley, T. S., Brennan, S. C., Yarova, P. L., Graca, J., Hanif, U.-K., Müller, C., Manhardt, T., Salzmann, M., Quasnichka, H., Price, S. A., Ward, D. T., Gilbert, T., Matchkov, V. V., Fenton, R. A., Herberger, A., Hwong, J., ... Riccardi, D. (2022). Impaired Mineral Ion Metabolism in a Mouse Model of Targeted Calcium-Sensing Receptor (CaSR) Deletion from Vascular Smooth Muscle Cells. *Journal of the American Society of Nephrology : JASN*, *33*(7), 1323-1340. https://doi.org/10.1681/ASN.2021040585, https://doi.org/10.1681/ASN.2021040585

Published in:
Journal of the American Society of Nephrology : JASN

Citing this paper
Please note that where the full-text provided on Manchester Research Explorer is the Author Accepted Manuscript or Proof version this may differ from the final Published version. If citing, it is advised that you check and use the publisher's definitive version.

General rights
Copyright and moral rights for the publications made accessible in the Research Explorer are retained by the authors and/or other copyright owners and it is a condition of accessing publications that users recognise and abide by the legal requirements associated with these rights.

Takedown policy
If you believe that this document breaches copyright please refer to the University of Manchester's Takedown Procedures [http://man.ac.uk/04Y6Bo] or contact uml.scholarlycommunications@manchester.ac.uk providing relevant details, so we can investigate your claim.

Download date:07. gen. 2025

Impaired mineral ion metabolism in a mouse model of targeted calcium-sensing receptor (CaSR) deletion from vascular smooth muscle cells.

Accepted author manuscript (not proofed, not copyedited; not updated).

The proofed and copyedited published version can be found at:

https://doi.org/10.1681/ASN.2021040585

https://jasn.asnjournals.org/content/early/2022/05/17/ASN.2021040585

Impaired mineral ion metabolism in a mouse model of targeted calcium-sensing receptor (CaSR) deletion from vascular smooth muscle cells

---

Martin Schepelmann[1,2], Marianna Ranieri[3], Irene Lopez-Fernandez[1], Thomas S. Webberley[1], Sarah C. Brennan[1,4], Polina L. Yarova,[1,5], Joao Graca[1,6], Umar-Khetaab Hanif[1], Christian Müller[2], Teresa Manhardt[2], Martina Salzmann[2], Helen Quasnichka[1], Sally A. Price[6], Donald T. Ward[7], Thierry Gilbert[8], Vladimir V. Matchkov[9], Robert A. Fenton[9], Amanda Herberger[10], Jenna Hwong[10], Christian Santa Maria[10], Chia-Ling Tu[10], Enikö Kallay[2], Giovanna Valenti[3], Wenhan Chang[10] and Daniela Riccardi[1].

1 School of Biosciences, Cardiff University, United Kingdom
2 Institute of Pathophysiology and Allergy Research, Medical University of Vienna, Austria
3 Department of Biosciences, Biotechnologies and Biopharmaceutics, University of Bari, Italy
4 Charles Perkins Centre, University of Sydney, NSW 2006, Australia
5 Translational & Clinical Research Institute, Newcastle University Medical School, Newcastle upon Tyne, UK
6 AstraZeneca, Macclesfield, Cheshire, United Kingdom
7 Division of Diabetes, Endocrinology & Gastroenterology, University of Manchester, Manchester, UK
8 Centre for Developmental Biology, University Paul Sabatier, Toulouse, FR
9 Department of Biomedicine, Aarhus University, Aarhus 8000, DK
10 Department of Medicine, University of California, San Francisco, CA, USA

Running title: Mineral ion dyshomeostasis in VSMC-CaSR knockout mice

Address correspondence to:

Wenhan Chang, PhD
University of California San Francisco
1700 Owens Street
San Francisco CA 94158, USA
Phone: (+1) 415-575-0558
Wenhan.Chang@ucsf.edu

Martin Schepelmann, PhD
Institute of Pathophysiology and Allergy Research
Medical University of Vienna
Währinger Gürtel 18-20, Leitstelle 3Q
1090, Vienna, Austria
Phone: (+43) 1 40400 51230
martin.schepelmann@meduniwien.ac.at

Daniela Riccardi, PhD
School of Biosciences
The Sir Martin Evans Building, Cardiff University
Cardiff CF10 3AX, United Kingdom
Phone: (44) (0) 29 208 79132
riccardi@cardiff.ac.uk

38 ## Significance statement

39 Chronic kidney disease (CKD) is associated with increased risk of mortality. In CKD, calcium
40 and phosphate dyshomeostasis are associated with altered expression of the calcium-sensing
41 receptor (CaSR) in the parathyroid glands and the kidney. The CaSR is also present in the
42 vasculature, but its contribution to total body mineral ion homeostasis is unknown. Here we
43 show that selective CaSR ablation from vascular smooth muscle cells (VSMC) leads to
44 profound mineral ion imbalance in mice. These results demonstrate a hitherto undiscovered
45 mode of mineral ion regulation outside the parathyroid glands and the kidneys. Alterations in
46 VSMC-CaSR expression and activity would be expected to contribute to mineral ion imbalance in
47 CKD.

48 ## Abstract

49 **Background:** Impaired mineral ion metabolism is a hallmark of chronic kidney disease (CKD)
50 -metabolic bone disorder. It can lead to pathological vascular calcification (VC) and is
51 associated with an increased risk of cardiovascular mortality. Loss of calcium sensing receptor
52 (CaSR) expression in vascular smooth muscle cells (VSMCs) exacerbates VC *in vitro*;
53 conversely, VC can be reduced by CaSR allosteric activators, calcimimetics.

54 **Methods:** To determine the role of the CaSR in VC, we characterized mice with targeted *Casr*
55 gene knockout (KO) in VSMC ($^{SM22\alpha}$CaSR$^{\Delta flox/\Delta flox}$).

56 **Results:** VSMC cultured from KO mice calcified more readily than those from control (WT)
57 mice i*n vitro*. However, KO mice did not show ectopic calcifications *in vivo* but a profound
58 mineral ion imbalance. Specifically, KO mice exhibited hypercalcemia, hypercalciuria,
59 hyperphosphaturia, and osteopenia, with elevated circulating FGF23, calcitriol (1,25-D_3), and
60 PTH levels. Renal tubular, but not vascular α-Klotho protein expression was increased in KO
61 mice. The observed phenotype of the KO mice could not be accounted for by altered CaSR
62 expression in the kidney or the parathyroid glands.

63 **Conclusions:** These results suggest that the VSMC-CaSR directly contributes to total body
64 mineral ion homeostasis, in addition to the established role of the receptor in the parathyroid-
65 kidney-bone axis.

66 ## Introduction

67 Vascular calcification (VC) is a major complication in chronic kidney disease-metabolic bone
68 disorder (CKD-MBD) and is an independent predictor of cardiovascular morbidity and
69 mortality[1]. During VC, pro-contractile vascular smooth muscle cells (VSMC) undergo
70 osteogenic transdifferentiation[2]. This process is exacerbated by altered mineral ion homeostasis
71 in CKD-MBD patients[3, 4]. The CaSR is the key regulator of serum ionized calcium levels, *via*
72 modulation of parathyroid hormone (PTH) secretion by the parathyroid glands (PTG) as well
73 as Ca^{2+} reabsorption in the kidney[5]. Allosteric CaSR activators, calcimimetics, reduce plasma
74 PTH and Ca^{2+} levels, decrease the prevalence of VC in animal studies of CKD[6, 7] and reduce
75 cardiovascular events in older patients with moderate to severe hyperparathyroidism receiving
76 hemodialysis[8]. However, the CaSR is also expressed in blood vessels where it may have a direct
77 protective role against VC. We and others have shown that in VSMC, the CaSR is
78 vasculoprotective, and that there is an inverse relationship between CaSR expression and VC[9,
79 10]. In uremic rats, administration of calcimimetics protects against VC[9-14]. CaSR expression is
80 lost in cultured VSMC kept under pro-calcifying conditions *in vitro* and in calcified human
81 arteries[9, 15] an effect which is, at least in part, restored by calcimimetic treatment[10, 12]. Over-
82 expression of a "dominant negative" CaSR mutation accelerates calcification of isolated
83 VSMC, which is prevented by calcimimetics[9]. However, there is a discrepancy between the
84 preclinical *in vitro* observations and clinical findings about the role of the CaSR in VC. For
85 instance, CaSR polymorphisms are not determinant of VC or cardiovascular outcomes in renal
86 transplant patients[16], suggesting that the protective cardiovascular effects of calcimimetics in
87 advanced CKD-MBD patients may also be modulated by additional systemic or local factor
88 like PTH, vitamin D, and FGF23. Thus, the precise contribution of the vascular CaSR to
89 pathological VC *in vivo* remains to be fully elucidated. To address this question directly, we
90 studied mice with targeted *Casr* gene ablation in VSMC, in which we have previously

91 demonstrated a significant role of the receptor in the regulation of blood pressure and vascular
92 tone[17].

93 ## Materials and Methods
94

95 ### Experimental animals

96 All animal procedures were approved by local ethical review and conformed with the
97 regulations of the UK Home Office and/or the Animal Care and Use Committees of all the
98 participating institutions. VSMC-specific CaSR knock-out mice were produced by breeding
99 $CaSR^{flox/flox}$ mice, which carry 2 loxP sequences flanking exon 7 of the *Casr* gene[18], with
100 SM22α (transgelin)-Cre mice. SM22α is transiently expressed during embryonic development
101 in cardiac myocytes and, by mid-gestation, is confined to visceral and vascular SMCs[19].
102 Genotyping, husbandry, *etc*. are described in[17, 20]. $^{SM22a}CaSR^{\Delta flox/\Delta flox}$ mice (VSMC-CaSR
103 knock-out, **KO**) and Cre-negative, $CaSR^{flox/flox}$ littermates (called "wild-type", for the wild-type
104 CaSR; **WT**) were used for all experiments. Male mice only were used for all experiments,
105 except for osmolality, soluble CaSR and bone metabolism marker measurements. All mice were
106 on the same C57Bl/6 genetic background.

107 ### Culture media

108 Dulbecco's modified Eagle medium (DMEM) without $CaCl_2$, containing 1 mM phosphate,
109 (Life Technologies, Grand Island, NY, USA) was supplemented with 1.2 mM $CaCl_2$, 50 U/ml
110 penicillin-streptomycin, 2 mM L-glutamine, 10 % (v/v) fetal bovine serum (FBS), 1 mM Na-
111 pyruvate and 1 % (v/v) amphotericin B solution (all Life Technologies) was used for the initial
112 isolation of VSMCs (growth medium). For further culturing, the same medium was used but
113 with omission of amphotericin B (culture medium). When indicated, the medium was
114 supplemented with different concentrations of Ca^{2+} and inorganic phosphate (Pi) *via* addition
115 of sterile 1M $CaCl_2$ solution and inorganic 1M phosphate buffer (NaH_2PO_4 / Na_2HPO_4) pH 7.4.

116 **Primary VSMC isolation**

117 VSMC were prepared according to published procedure[21] with modifications. In brief, mice
118 were killed by cervical dislocation and the thoracic aorta was dissected. Aortas of 2-5 mice of
119 the same genotype were pooled for one cell isolation and placed in growth medium and cleaned
120 from the tunica adventitia and connective tissue. Segments of aorta ca. 1 mm in length were
121 transferred to a culture flask and, after 10 minutes of drying / attaching in a tissue culture
122 incubator, covered with growth medium and incubated at 37 °C / 95 % relative humidity / 5 %
123 CO_2 until cells had grown out of the explants (ca. 2-4 weeks). The explants were then removed
124 by aspiration and the cells were passaged using 0.05 % (v/v) trypsin-ethylenediaminetetraacetic
125 (EDTA) solution in sterile phosphate-buffered saline, pH 7.4 (PBS) without $CaCl_2$ and $MgCl_2$
126 (all Life Technologies). Beginning with this passage VSMC culture medium was used instead
127 of growth medium. Medium was changed every 3-4 days. Cells were used for experiments at
128 passages 2-6. See **Figure S1** for a photograph array of the procedure.

129 **Immunohistochemistry**

130 Mouse organs were fixed by immersion in 4 % (w/v) paraformaldehyde (PFA) in PBS for 4
131 hours and 4 µm paraffin sections were cut and rehydrated according to standard protocols.
132 Immunostainings were carried out to detect CaSR (1:500, MA1-934, Thermo Scientific,
133 Loughborough, UK), TRPV5 (1:400, Alomone Labs, Jerusalem, Israel), Calbindin D-28k
134 (1:3000, Sigma-Aldrich, Gillingham, UK), and PMCA 1/4 (1:100, Santa Cruz Biotechnology,
135 Santa Cruz, USA). These immunostainings were carried out using a Ventana XT autostainer
136 and OmnimapTM DAB reagents (Ventana, Tucson, USA). Hematoxylin (Clin-Tech,
137 Guildford, UK) was used to counterstain the tissue sections, which were then dehydrated in
138 ethanol, cleared in xylene, and mounted using Hystomount (TAAB Labs, Aldermaston, UK) or
139 Fluoromount G (Thermo Fisher). Cyp27b1 and α-Klotho protein in aortas was detected using
140 rabbit anti-Cyp27b1 (1:500, LSBio, Seattle, USA) and rabbit anti-klotho (1:200, Abcam)

141 antibodies, respectively. Antigen retrieval was performed by incubation for 20 min in 10 mM
142 citrate buffer pH 6 in a steamer. Bound antibodies were visualized using the Dako Envision+
143 HRP rabbit kit (Agilent, Santa Clara, USA), nuclei were counterstained using Haematoxylin
144 and mounted in Fluoromunt G. Tissue slides were scanned using a Scanscope® scanner (Aperio
145 Technologies Incorporated, Vista, USA) or TissueFAXS Hard- and Software (TissueGnostics
146 GmbH, Vienna, Austria). Quantitative evaluation of immunohistochemichal stainings was
147 performed using ImageJ[22, 23], where % positive cells / positive area was counted after manual
148 thresholding. For the aorta sections, mean color value for endothelium and smooth muscle layer
149 were measured by subtracting the values of the negative controls for each aorta (IgG control)
150 from the positively stained sections.

151 **Immunofluorescence**

152 Dissected organs were fixed by immersion in 4 % (w/v) PFA in PBS for 4 hours and then
153 washed in PBS and stored in 30 % (w/v) sucrose in PBS at 4 °C for cryosections or dehydrated
154 and paraffin embedded for paraffin sections. For cryosections, tissues were embedded in
155 optimal cutting temperature compound (TissueTek OCT, Sakura-Finetek, Alphen aan den Rijn,
156 NL) on dry ice and 8-10 µm sections were prepared using a cryo-microtome (Leica 2300L,
157 Leica microsystems, Milton Keynes, UK). Rehydrated sections were incubated for 10 minutes
158 in 50 mM NH_4Cl in PBS and then were antigen retrieved in 10 mM citrate buffer pH 6 for 15
159 minutes in a steamer followed by 5 minutes in 1 % sodium dodecyl sulphate (SDS) in PBS.
160 Non-specific antibody binding was prevented by incubation in 1 % (w/v) BSA + 0.1 % (v/v)
161 Tween 20 in PBS (blocking buffer) for 1 hour at room temperature. The CaSR was labelled by
162 incubating the sections overnight with a rabbit-derived polyclonal antibody (1:100; AnaSpec,
163 53286, Fremont, CA, USA) or a mouse derived monoclonal antibody (1:500, clone 5C10,
164 Abcam) in blocking buffer. Negative controls were performed by omission of the primary
165 antibodies or replacement with an isotype control of rabbit IgG (Abcam). After washing in PBS,

166 primary antibody binding was visualized using appropriate Alexa Fluor fluorescence-dye
167 coupled secondary anti IgG antibodies in a dilution of 1:500 in blocking buffer. High
168 background was quenched by incubation of the sections in 0.2 mM Sudan Black B in 70 %
169 ethanol for 10 minutes after the secondary antibody[24]. Nuclei were counterstained with Hoechst
170 34580 and slides were mounted using ProLong Gold® (all Life Technologies).

171 ***In vitro* calcification assays**

172 Cells were seeded in 24-well plates and were grown to 100 % confluency. The medium was
173 then changed to growth medium supplemented with various $CaCl_2$ concentrations as specified
174 in the results section. For induction of calcification, Pi (in the form of 1 M Na-phosphate buffer
175 pH 7.4) were added to the culture medium. Cells were left in culture for 10 days and then fixed
176 for 15 minutes in 4 % (w/v) PFA at room temperature. The amount of calcification was
177 visualized by staining with 2 % alizarin red S (w/v) in water, pH 4.3, as described[25]. For
178 quantification, after the incubation period, the cells were washed twice in PBS for and deposited
179 calcium was extracted by decalcifying overnight in 0.6 N HCl at 37 °C. Eluted Ca^{2+}
180 concentration was measured using the o-cresolphthalein complexone method[26, 27] and
181 normalized against total protein concentration of the lysed cells (Pierce BCA assay; Thermo
182 Fisher Scientific).

183 ***Ex vivo* calcification of aortic explants**

184 The assay was performed as described elsewhere[28]. In brief, aortas were dissected as described
185 for the primary VSMC isolation. After cleaning the aortas from tunica adventitia, the
186 endothelial layer was destroyed by stretching the tissue over the whole length. The vessel was
187 then cut into 3-4 pieces of approximately equal length (5–8 mm). The pieces were incubated
188 for 5 days in growth medium supplemented with varying of $CaCl_2$ concentrations (1.2–2.5 mM)
189 and 3 mM inorganic phosphate, similarly to the VSMC calcification assays. Ca^{2+} concentrations
190 were measured by o-cresolphthalein complexone method as described above and normalized

191 against the weight of the explants. Typical explant weights varied between 1.0 and 5.0 mg.
192 Cryosections of 4 % (w/v) PFA fixed WT and KO aortas were stained for calcifications using
193 Alizarin Red S as described above.

194 Parathyroid isolation and *ex vivo* PTH secretion

195 The *ex vivo* PTH-secretion assay in cultured mouse PTGs was adapted from[29]. Briefly, two
196 mouse PTGs cleaned from surrounding tissues were submerged in a micro-droplet (10 µl) of
197 secretion medium [SM, MEM Eagles with Earle's balanced salts supplemented with 0.5 mM
198 Mg, 0.2 % bovine serum albumin, and 20 mM HEPES (pH 7.4)] and placed in the center of a
199 13 mm track-etched (0.1 µM pore) polycarbonate (PC) membrane, floating on a large drop (0.5
200 ml) of ice-cold SM supplemented with 3.0 mM Ca^{2+}. When all glands for the same experiment
201 were dissected out, the PC membranes carrying the glands were transferred onto fresh drops of
202 37 °C SM containing 0.5 mM Ca^{2+} and equilibrated for ~45 minutes. Afterwards, the membrane
203 with each pair of glands was transferred sequentially to a fresh drop (500 µl) of SM at 37 °C,
204 increasing the Ca^{2+} concentration in the medium from 0.5 to 3.0 mM with 60 min for each
205 concentration and a fresh medium change midway (at 30 minutes). Intact PTH released into the
206 culture media was determined by ELISA (Quidel, San Diego, USA) in duplicate and used to
207 calculate the rate of PTH release. For Ca^{2+} set-points, rates of PTH release were normalized to
208 the rate at 0.5 mM Ca^{2+} and plotted against the Ca^{2+} concentration, and the PTH set-points (=
209 EC_{50}) were deduced from the curve as the Ca^{2+} concentration which inhibits 50 % of the Ca^{2+}-
210 suppressible PTH release.

211 Microcomputed tomography (µCT)

212 µCT was performed on distal femur for trabecular (Tb) bone and tibio-fibular junction (TFJ)
213 for cortical (Ct) bone as described[29]. Briefly, femurs and tibiae fixed in 10 % phosphate-
214 buffered formaldehyde (PBF) were scanned by a SCANCO vivaCT 100 scanner (SCANCO
215 Medical AG, Basserdorf, Switzerland) with 10.5 µm voxel size and 55 kV X-ray energy. For

216 Tb bone in the distal femoral metaphysis, 100 serial cross-sectional scans (1.05 mm) of the
217 secondary spongiosa were obtained from the end of the growth plate extending proximally. For
218 Ct bone, 100 serial cross-sections (1.05 mm) of the tibia were obtained from the TFJ extending
219 proximally. A threshold of 420 mg hydroxyapatite (HA)/mm^3 was applied to segment total
220 mineralized bone matrix from soft tissue. Linear attenuation was calibrated using a µCT HA
221 phantom. µCT image analysis and 3D reconstructions were done using the manufacturer's
222 software to obtain the following structural parameters: Tb tissue volume (Tb.TV), Tb bone
223 volume (Tb.BV), Tb.BV/TV ratio, Tb number (Tb.N), Tb connectivity density (Tb.CD), Tb
224 thickness (Tb.Th), Tb spacing (Tb.Sp), Ct tissue volume (Ct.TV), and Ct thickness (Ct.Th).

225 **Nephron count**

226 One kidney per adult animal (16 weeks) was removed, decapsulated and immersed in 6M HCl
227 at 37°C for 35 minutes. After several washes with tap water, the macerated kidney was stored
228 at 4°C overnight. The tissue was homogenized with a glass-stirring rod and transferred to a 50
229 ml volumetric flask. Tap water was added to adjust the volume and the tubules and glomeruli
230 suspension was then ready for nephron counting. One 0.5 ml aliquot was taken and deposited
231 onto a glass slide with a millimeter mesh lattice to count the number of glomeruli. The total
232 number of nephrons per kidney was calculated using the mean of 3 to 4 counts.

233 **Tissue preparation for Western blot and RT-qPCR experiments**

234 Mouse kidney slices were prepared as previously described[30]. In brief, WT and KO mice were
235 euthanized by cervical dislocation. Kidneys were quickly removed and about 500 µm sections
236 were made. Sectioned kidneys were equilibrated for 10 min in a specific kidney-slice buffer
237 that contained 118 mM NaCl, 16 mM HEPES, 17 mM Na-HEPES, 14 mM glucose, 3.2 mM
238 KCl, 2.5 mM $CaCl_2$, 1.8 mM $MgSO_4$, and 1.8 mM KH_2PO4 (pH 7.4) at 37°C. For Western
239 blotting experiments, sections were then homogenized with a mini-potter in ice-cold kidney-
240 slice buffer and Halt™ protease and phosphatase inhibitor Cocktail (Thermo Fisher, Rockford,

241 USA). Suspensions were centrifuged at 12,000 x *g* for 10 min at 4°C, and supernatants were
242 loaded on acrylamide gels. Bones were prepared from hind-leg bones (femur, tibia and fibia)
243 after cleaning of the surrounding connective tissue. After cleaning of the aortas from the tunica
244 adventitia, the vessel was cut into 3-4 pieces, which were then processed accordingly.
245 For RT-PCR experiments, total RNA was extracted from kidneys, aorta and bones using Trizol
246 reagent according to the manufacturer's instructions (Invitrogen, Life Technologies, Monza,
247 Italy).

248 **Gel Electrophoresis and Immunoblotting**

249 Proteins were separated on 8-13 % bis-tris acrylamide gels under reducing conditions. Protein
250 bands were electrophoretically transferred onto Immobilon-P membranes (Millipore Corporate
251 Headquarters, Billerica, USA) for Western blot analysis, blocked in TBS-Tween-20 containing
252 3 % bovine serum albumin (BSA) and incubated with primary antibodies overnight.
253 Antibodies: polyclonal rabbit anti-CaSR (AnaSpec, this antibody had previously been
254 determined to be most suitable for mouse tissue[31]), polyclonal rabbit anti-AQP2 (raised against
255 20-amino acids at the N-terminal, custom made from the polyphosphorylated region of rat
256 AQP2)[32], polyclonal rabbit anti-AQP2-pS256 (a gift from Peter Deen)[33], polyclonal rabbit anti-
257 AQP2-pS261 (Novus Biologicals, Littleton, Colorado, USA), polyclonal antibody against
258 NaPi2a (Alpha Diagnostic Intl. Inc, San Antonio, Texas, USA), polyclonal rabbit anti-Klotho
259 (Abcam, Cambridge, UK), monoclonal mouse anti-NCC (StressMarq Biosciences Inc.,
260 Victoria, CDN), polyclonal rabbit anti-β-actin (Cell Signaling Technology, Leiden, NL) and
261 rabbit antibodies raised against the last 10 C-terminal amino acids (C-GANANRKFLD) of the
262 E subunit of the V-ATPase (a gift from Dr Dennis Brown, Harvard Medical School, Boston,
263 MA, USA). Secondary goat anti-rabbit or goat anti-mouse horseradish peroxidase–coupled
264 antibodies were obtained from Santa Cruz Biotechnologies (Tebu-Bio, Milan, IT). Membranes
265 were developed using Super Signal West Pico Chemiluminescent Substrate (Pierce, Rockford,

266 USA) with Chemidoc System (Bio-Rad Laboratories, Milan, Italy). Densitometry analysis was
267 performed using Image Lab from Bio-Rad Laboratories, Inc. (Hercules, California, USA).

268 **Real-Time PCR**

269 Real-Time PCR experiments were performed to measure the relative expression of mRNA from
270 WT and KO mouse kidneys, aorta, and bone. Total RNA was extracted using Trizol (Invitrogen,
271 Life Technologies, Monza, Italy). Reverse transcription was performed on 1 µg of total RNA
272 using SuperScript VILO Master Mix (Invitrogen, Life Technologies, Monza, Italy). Real-time
273 PCR amplification was performed using TaqMan® Fast Advanced Master Mix with Aqp2 (ID
274 number: Mm00437575_m1), CaSR (ID number: Mm00443375_m1), α-Klotho (ID number:
275 Mm00502002_m1), NaPi2a (ID number: Mm00441450_m1), Tagln or Sm22α (ID number:
276 Mm00441661_g1), FGF23 (ID number: Mm00445621_m1) and CYP27B1 or 1α-hydroxylase
277 (ID number: Mm01165918_g1) assay, using GAPDH (ID number: Mm99999915_g1) and 18S
278 (ID number: Hs99999901_s1) assay as housekeeping genes (Applied Biosystem, Life
279 Technologies, Monza, Italy) in a StepOne Real-Time PCR System (Applied Biosystem, Life
280 Technologies, Monza, Italy). Results were calculated according to the ΔΔCt method as relative
281 expression to the average gene expression in the WT samples and then calculated as fold
282 changes via $2^{-\Delta\Delta Ct}$.

283 **Blood and urine collection, metabolic cages**

284 Post-mortem blood collection from animals after neck dislocation was performed *via* cardiac
285 puncture or retro-orbitally. Blood collection from live animals was performed *via* tail nick, as
286 described [34]. K-EDTA, Na-heparin plasma and serum were collected in respective tubes (BD
287 Biosciences, Oxford, UK). The blood was then centrifuged at 2,000 x *g* for 10 minutes and the
288 supernatant stored at -80 °C. For urine collection, mice were weighed and transferred to
289 metabolic cages (Tecniplast, Buguggiate, IT) and then left for 48 hours to allow them to
290 acclimatize to the new environment. Mouse weight, food and water intake, as well as feces and

291 urine production were recorded over a period of 4 days. Samples from day 3 and 4 were then
292 used for urine analysis and the results for both days were averaged. Urine was stored at -80 °C
293 for further analysis.

294 **Blood and urine analysis**

295 Commercially available assays were used to measure plasma concentrations of Fetuin A (R&D
296 Systems, Abingdon, UK), pyrophosphate (Abcam), FGF 23 (Kainos Laboratories, Tokyo,
297 Japan), 1–84 PTH (Immutopics, San Clemente, USA), calcitriol (1,25-D_3) (Immunodiagnostic
298 Systems, Tyne & Wear, UK), P1NP (Immunodiagnostic Systems), and TRAcP5b
299 (Immunodiagnostic Systems), as well as serum concentration of soluble CaSR / N-terminal
300 CaSR fragment (Elabscience, Wuhan, CN), and α-Klotho (cloud Clone Corp., Wuhan, CN).
301 Concentrations of electrolytes were analyzed using a Roche modular P analyzer (Roche
302 diagnostics) or, as were urea, creatinine, uric acid, glucose, and protein, by a commercially
303 available clinical pathology service (MRC Harwell, Oxford, UK). Serum osmolality was
304 measured using an Osmomat 30 (Gonotec, Berlin, DE) freezing point depression osmometer.
305 Electrolyte concentrations for urine are reported as ion:creatinine ratio (abbreviated as ion:Cr),
306 other clinical urine biomarkers (creatinine, total protein, urea and uric acid) are reported as
307 excreted amount per day and total body weight (TBW). Urine osmolality was measured using
308 a VAPRO® vapor pressure osmometer 5520 Wescor Inc., (Puteaux, France). Urine pH was
309 measured using litmus paper with a range of pH between 2.0 and 9.0 (Macherey-Nagel, Düren,
310 Germany). For urine precipitated analysis, 20 µl of urine were placed on the glass slide and
311 covered with a coverslip. Samples were studies with phase contrast microscopy and analyzed
312 qualitatively. Urinary AQP2 excretion was measured by ELISA as previously described[35, 36].

313 **Statistical Analysis**

314 All statistical analyses were performed using GraphPad Prism 8 (GraphPad Software, La Jolla,
315 CA, USA). Statistical sample size is reported as N (number of separate experiments / biological

316 repeats) over n (technical repeats per sample, where applicable). Data are generally presented
317 as mean ± SD, except for RT-qPCR data, which are shown as median ± interquartile range.
318 A difference of $p<0.05$ was considered statistically significant. The employed statistical tests
319 and significance levels are specified in the respective results sections or in the figure legends.

320 Results

321 CaSR ablation induces calcification of VSMC *in vitro* but not *ex vivo* or *in vivo.*

322 Effectiveness of CaSR ablation from VSMC of $^{SM22\alpha}$CaSR$^{\Delta flox/\Delta flox}$ mice, at the molecular and
323 functional levels, had already been confirmed previously[17, 37]. To test directly whether CaSR
324 ablation prompts VSMCs to calcify, VSMC isolated from WT and KO mice were cultured in
325 rising concentrations of Ca^{2+} (0.8–2.2 mM) and inorganic phosphate (Pi, 2–3 mM), spanning
326 the (patho)physiological range. WT VSMC showed no calcification at 2 mM Pi at any Ca^{2+}
327 concentration, while at 3 mM Pi, calcification was seen at ≥1.6 mM Ca^{2+}. In VSMC derived
328 from KO aortae, calcification was significantly greater, and was already observed in 2 mM Pi
329 at 1.6 mM Ca^{2+} or in 3 mM Pi at 1.2 mM Ca^{2+} (**Figure 1A**). Ca^{2+} incorporation in VSMC was
330 Ca^{2+}-concentration dependent and was markedly more pronounced in VSMC from KO than in
331 those from WT mice (**Figure 1B**). Furthermore, VSMC from WT and KO mice were cultured
332 in 3 mM Pi and only 1.2 mM Ca^{2+}, so as to not saturate CaSR-activation, but in combination
333 with 10 nM of the calcimimetic R-568. R-568 reduced calcium incorporation only in WT but
334 not KO VSMC when compared to vehicle control (**Figure 1C**). Together, these results
335 confirmed that the CaSR protects *in vitro* VSMC calcification.
336 Based on these observations, we had expected the KO mice to develop calcification in their
337 blood vessels. However, there was no evidence of increased *in vivo* Ca^{2+} incorporation in the
338 aortas of three-month-old KO mice compared to age matched WT controls. *Ex vivo* whole aortic
339 explants from both six-month-old KO and WT mice, kept for ten days in 3 mM Pi and 1.8 mM

340 Ca^{2+} did not show any traceable calcification by alizarine red staining (**Figure S2**) and/or µCT
341 (data not shown). Finally, as shown previously, aortas from up to 12-month-old WT and KO
342 mice were histologically comparable and devoid of calcium deposits[17].
343

344 **$^{SM22\alpha}$CaSR$^{\Delta flox/\Delta flox}$ mice exhibit impaired mineral ion homeostasis and alterations**
345 **in calciotropic and phosphotropic hormones.**

346 ***Blood biochemistry***

347 Measurement of blood parameters, as shown in **Table 1**, showed moderate hypercalcemia and
348 elevated plasma FGF23, PTH and 1,25-D_3 levels in 3-month-old mice. FGF23 and Ca^{2+} levels
349 were also measured and found to be elevated in 18-month-old mice (**Table S1**) indicting that
350 the mineral ion imbalance persists throughout the lifespan of the KO mice, without any apparent
351 detrimental impact on their health. Serum α-Klotho-levels were comparable between both
352 genotypes, at 3- and 18-months of age, although older mice had higher mean α-Klotho-levels
353 than the younger ones.
354 Plasma Pi concentrations were reduced in 3-month-old KO compared to WT animals while
355 Na^+, K^+, Cl^- and Mg^{2+} levels, and the levels of the physiological inhibitors of calcification,
356 inorganic pyrophosphate (PPi) and Fetuin A were comparable between genotypes. Serum
357 albumin levels were slightly decreased (pointing also towards a higher proportion of free
358 ionized Ca^{2+} levels) while alkaline phosphatase (ALP) levels were increased in KO animals.
359 Kidney function and hydration appeared to be normal in KO mice as urea and blood urea
360 nitrogen (BUN), as well as hematocrit, did not differ from those of WT animals, while serum
361 creatinine was slightly reduced in KO animals (**Table 1**). Serum osmolality assessed in the 18-
362 month-old animals was unchanged between the two genotypes (**Table S1**). We also detected
363 no difference in the concentration of "soluble" CaSR or rather N-terminal CaSR fragment
364 between the genotypes in sera of 18-month-old animals (**Table S1**) which was comparable to

365 the level seen in serum of a 14-month-old non-genetically modified control (Ctrl) mouse.
366 "Soluble" CaSR was around the lowest detection limit in sera of 3-month-old animals (**Figure**
367 **S8**). These results exclude an antagonistic or hormonal effect of the truncated CaSR (encoded
368 by exons 2-6) as the cause for the observed phenotype.
369

370 ***Metabolism, urine and organ weight***

371 Urinary Ca^{2+}:Cr and Pi:Cr levels of KO were strongly elevated compared to WT animals (7.2-
372 fold and 2.9-fold respectively), while Na^{+}:Cr, K^{+}:Cr, Cl^{-}:Cr and Mg^{2+}:Cr, creatinine, total
373 protein, urea, uric acid, and glucose excretion ratios were comparable between the genotypes
374 (**Table 2**). No differences in food consumption or fecal output were observed between
375 genotypes. Water consumption and urine excretion were non-significantly elevated in KO mice
376 compared to WT (**Table 2, Figure S3**).
377

378 ***Mineral ion and hormonal imbalance seen in $^{SM22\alpha}CaSR^{\Delta flox/\Delta flox}$ mice is not a direct***
379 ***consequence of altered gene/protein expression in the vasculature (aorta).***

380 The observed phenotype points to a profound mineral ion dyshomeostasis in KO mice. We
381 therefore investigated the expression of α-Klotho and 1α-hydroxylase since they are powerful
382 regulators of mineral ion metabolism. mRNA expression of *α-Klotho*, *Cyp27b1*, and the smooth
383 muscle marker *sm22α* were unchanged between WT and KO animals. CYP27B1 and α-Klotho
384 protein expression levels were comparable between genotypes in both the endothelium and
385 smooth muscle layers of the aorta (**Figure 2**). The cause of the observed mineral ion and
386 hormonal imbalance in KO mice must therefore lie elsewhere.
387

388 ***$^{SM22\alpha}CaSR^{\Delta flox/\Delta flox}$ mice exhibit altered expression of renal α-Klotho and of Ca^{2+} and Pi***
389 ***transport proteins.***

390 Renal expression of α-Klotho protein was significantly increased while that of the proximal
391 tubule Na^{+}-dependent Pi transporter NaPi2a was significantly decreased in the kidneys of KO
392 mice. The number of vitamin D receptor positive cells over whole kidney sections as
393 determined by semi-quantitative immunohistochemistry analysis was comparable between
394 genotypes, as was the mRNA expression of *Cyp27b1* (**Figure 3 and Figure S4**). The elevated
395 plasma levels of 1,25-D_3 seen in KO mice could not be explained by the unchanged CYP27B1
396 protein expression in the kidney, which was comparable between genotypes (**Figure S5**),
397 indicating extrarenal sources of 1,25-D_3. In supporting the action of 1,25-D_3 to increase urinary
398 Ca^{2+} reabsorption[38], the expression of the epithelial Ca^{2+} channel TRPV5, the cytosolic Ca^{2+}
399 buffer calbindin D28K, and the basolateral plasma membrane Ca^{2+}-ATPase (PMCA) was
400 significantly increased in kidneys from KO compared to WT mice, as indicated by the larger
401 area where staining intensities were above the threshold level (**Figure 3**).
402 Next, we confirmed that CaSR ablation from VSMC did not yield altered CaSR expression or
403 gross anatomical changes in the kidney which could account for the observed phenotype. Renal
404 CaSR mRNA and protein expression and distribution pattern (**Figure 3**, **Figure S6)** were all
405 comparable between genotypes. There were no histomorphological differences between the
406 kidneys of WT and KO mice of comparable age (**Figure S6A, B**). Kidney weights were
407 comparable between WT and KO animals, both at 6 and 18 months of age (**Table S2**), as were
408 nephron numbers (WT 30.54±5.21 *vs* KO 31.63±4.80 nephrons/mg kidney, mean±SD, N=7).
409 Other organ weights (liver, stomach, spleen) were similar between genotypes, except for the
410 hearts of 18-month-old KO animals, which were slightly heavier than those of age-matched WT
411 animals (**Table S2**).
412

413 ***Urinary crystals, dilution and aquaporin expression levels of $^{SM22\alpha}CaSR^{\Delta flox/\Delta flox}$ mice.***

414 The observed hypercalciuria and hyperphosphaturia could promote renal stone formation.
415 While overt nephrolithiasis or nephrocalcinosis were not detected by histopathology, we did
416 observe micro crystals in the urine of KO, but not WT animals (**Figure 4A**). Urine of KO mice
417 had significantly reduced osmolality and pH compared to WT controls (**Figure 4**). The
418 expression of the apical thiazide-sensitive Na^{+}-Cl^{-} cotransporter (NCC) and of the V-type H^{+}
419 ATPase were significantly increased in KO mouse kidneys, potentially leading to increased
420 NaCl reabsorption and urine acidification respectively. Accordingly, the expression of the
421 aquaporin-2 water channel (total AQP2) was significantly reduced in the kidneys of KO mice
422 at both the mRNA and protein levels (**Figure S4** and **Figure 4F**). Specifically, the expression
423 of the proteasome-sensitive phosphorylated form of AQP2, pS261[39], was upregulated while the
424 active, vasopressin-stimulated pS256-AQP2[35] was downregulated in KO mice (**Figure 4G, H**),
425 indicating a decreased amount of functional AQP2 resulting in decreased renal concentrating
426 ability. In addition, urinary excretion of AQP2 was increased in KO animals (**Figure 4I**),
427 pointing towards a higher degree of AQP2 degradation. Overall, KO mice had reduced urine
428 concentrating ability, possibly as compensation to prevent kidney stone formation.

429

430 ***Hyperparathyroidism of $^{SM22\alpha}CaSR^{\Delta flox/\Delta flox}$ mice is neither due to altered CaSR expression,***
431 ***nor function, in the PTG.***

432 VSMC-CaSR KO mice exhibit hypercalcemia and mild hyperparathyroidism (to reiterate,
433 plasma total Ca^{2+}: 2.28 mmol / l *vs.* 2.94 mmol / l and PTH 151.7 *vs.* 256.6 pg/ml, WT *vs.* KO,
434 see **Table 1**).To investigate whether the observed phenotype was due to partial ablation of the
435 parathyroid CaSR, possibly through *SM22a* promoter leakage, we characterized CaSR
436 expression and PTG function in the KO animals. PTGs from WT and KO animals were
437 comparable in size and morphology (**Figure 5A**), as was the glands' CaSR expression (**Figure**

438 **5B and C**). Similarly, isolated PTGs had overlapping PTH secretion curves in response to rising
439 levels of extracellular Ca^{2+} for both genotypes with identical IC_{50} values of ~ 1.1 mM Ca^{2+}_o
440 (**Figure 5D**). Thus, the profound changes in mineral ion homeostasis seen in KO animals cannot
441 be accounted for by altered CaSR expression, or function, in the PTGs.
442

443 ***^{SM22a}CaSR$^{\Delta flox/\Delta flox}$ mice exhibit elevated bone FGF23 levels and osteopenia.***

444 The increased circulating levels of the phosphaturic hormone FGF23 are, at least in part, of
445 skeletal origin, as FGF23 mRNA expression levels were increased in bones of KO mice (**Figure**
446 **S7**). In contrast, FGF23 mRNA was undetectable in blood vessels of both genotypes (no
447 amplification).
448 Micro-computerized tomography (µCT) on hind-leg bones of 3-month-old WT and KO mice
449 revealed that especially trabecular bone quality was significantly reduced in KO animals
450 compared to WT **(Table 3, Figure S7)**. These findings are in line with a significant increase in
451 plasma levels of the bone resorption marker tartrate-resistant acid phosphatase 5b (TRAcP5b)
452 in KO compared to WT animals, while the bone formation marker procollagen type 1 (P1NP)
453 was comparable in both genotypes (**Figure S7**).

454 Discussion

455 Our data suggest that the CaSR protects VSMC from calcification *in vitro,* though loss of the
456 VSMC-CaSR is apparently unable to induce detectable VC *in vivo*. Our mouse model further
457 demonstrated that the VSMC-CaSR contributes directly to the regulation of mineral ion
458 homeostasis, possibly by direct control of FGF23 and 1,25-D3 production / secretion, or
459 indirectly through influencing the calcium-sensing or hormonal resistance in calciotropic
460 organs. Most likely, the phenotype of the ^{SM22a}CaSR$^{\Delta flox/\Delta flox}$ mouse is the result of a
461 combination of disturbances acting together (**Figure 6**).

Vascular and VSMC calcification

VC is an independent predictor of cardiovascular morbidity and mortality in CKD-MBD patients[40, 41]. Previous observations in cultured human and bovine VSMC[9] indicated a direct role for the CaSR in preventing VSMC calcification / VC, which is substantiated by our findings on the effect and ability of CaSR ablation and calcimimetics to enhance and prevent VSMC calcification *in vitro*, respectively. These observations suggest that calcimimetics used clinically to treat patients with end-stage renal disease may reduce VC by directly targeting the vascular CaSR in addition to its action of improving mineral ion metabolism. However, the absence of VC in the aortae of KO mice *in vivo,* despite the animals' hypercalcemia, suggests that loss of CaSR expression is not sufficient to drive pathological VC.

An increase in 1α-hydroxylase expression in the vasculature promotes VC[42] but 1α-hydroxylase expression in the aortas of $^{SM22a}CaSR^{\Delta flox/\Delta flox}$ mice is not affected. High serum Pi levels are associated with greater prevalence of VC in patients with moderate CKD[43] whereas the $^{SM22a}CaSR^{\Delta flox/\Delta flox}$ were hypophosphatemic. Together with unchanged fetuin A and pyrophosphate (PPi) levels, potentially in combination with factors such as reduced vascular resistance in these animals[17], this may explain the lack of *in vivo* VC of $^{SM22a}CaSR^{\Delta flox/\Delta flox}$ mice.

Mineral ion metabolism imbalance

In addition to the previously described phenotype of reduced vascular contractility[17] and the changes in VSMC calcification behavior discussed above, we found that the $^{SM22a}CaSR^{\Delta flox/\Delta flox}$ mice also showed dysregulated mineral ion imbalance, manifesting in hypercalcemia, hypophosphatemia, hypercalciuria, hyperphosphaturia, and elevated FGF23, PTH, and 1,25-D_3 levels, together with increased bone resorption that is probably due to the chronically elevated PTH levels.

485 ***The phenotype is a direct consequence of VSMC-specific CaSR deletion***

486 CaSR expression and / or function in PTG and kidney was not affected in the $^{SM22a}CaSR^{\Delta flox/\Delta flox}$
487 mice. Indeed, the phenotype of these mice cannot be explained by off-target CaSR deletion
488 induced by our knock-out strategy, as constitutive or calciotropic organ specific CaSR deletion
489 have very different phenotypes (**Table 4**). The global CaSR knock-out mouse exhibits severe
490 hyperparathyroidism, growth retardation, and rarely lives longer than a few weeks[44] while the
491 $^{SM22a}CaSR^{\Delta flox/\Delta flox}$ mice grow normally and have a normal lifespan. Using our strategy (Δexon
492 7), targeted deletion of the CaSR from the PTG was shown to induce a severe phenotype of
493 hypercalcemia and hyperparathyroidism (~20-fold higher compared to controls)[18], along with
494 PTGs whose secretion are totally unresponsive to rising Ca^{2+} concentrations[45]. The PTGs of the
495 $^{SM22a}CaSR^{\Delta flox/\Delta flox}$ mice however were as responsive to extracellular Ca^{2+} as those from WT
496 mice. A similar strategy (Δexon 3) was used to specifically delete the CaSR from the kidney,
497 and these mice exhibit normal serum biochemistries and hypocalciuria[46]. Off-target effects of
498 the truncated amino terminus of the CaSR are also highly unlikely, given that circulating levels
499 of the (truncated) receptor were extremely low which would not be expected to interfere with
500 the millimolar extracellular Ca^{2+} concentration, and that the residual truncated protein is by
501 itself inactive and does not hinder the function of the native CaSR[18]. Collectively, these
502 considerations suggest that the observed phenotype can only be reasonably accounted for by
503 CaSR ablation from VSMC.

504 ***Features of the phenotype likely to be secondary to disturbed hormone secretion***

505 The hypercalcemia of the $^{SM22a}CaSR^{\Delta flox/\Delta flox}$ mouse is most likely downstream to the increase
506 in PTH and particularly 1,25-D_3 levels whereas the observed hypercalciuria is likely secondary
507 to the hypercalcemia. $^{SM22a}CaSR^{\Delta flox/\Delta flox}$ mice also showed hyperphosphaturia and
508 hypophosphatemia, likely *via* FGF23 and PTH induced down-regulation of NaPi2a and thus
509 decreased phosphate reabsorption from the urine. The mildly increased PTH levels are also

510 plausibly the cause for reduced bone mineral density together with an increase in the bone
511 resorption in the $^{SM22a}CaSR^{\Delta flox/\Delta flox}$ mice.

512 The underlying regulatory schemes become more complex when looking at the hormones
513 themselves. The increase in 1,25-D_3 production could be secondary to the increase in PTH,
514 though the hyperparathyroidism seems quite mild for such an effect. Also, given that the higher
515 serum Pi would be expected to limit CaSR activation[47] by extracellular Ca^{2+}, the hypercalcemia
516 and hypophosphatemia seen in the $^{SM22a}CaSR^{\Delta flox/\Delta flox}$ mice would provide optimal conditions
517 for enhanced CaSR activation in the parathyroid and thus reduced PTH secretion, instead of
518 hyperparathyroidism. These observations along with the unaltered Ca^{2+}-set point of PTH
519 secretion from KO PTGs suggest that loss of CaSR in VSMC influences other mechanisms to
520 promote PTH release *in vivo*.

521 The increase in 1,25-D_3 and PTH could then contribute to the elevated circulating FGF23 levels
522 which are, at least in part, of skeletal origin given that FGF23 mRNA was undetectable in the
523 aorta but was increased in the bones of $^{SM22a}CaSR^{\Delta flox/\Delta flox}$ mice.

524 ***Features of the phenotype likely to be caused by end-organ resistance***

525 1,25-D_3 is a potent inducer of FGF23[48] and, conversely, FGF23 reduces the production of 1,25-
526 D_3 by downregulating 1α-hydroxylase[49, 50] and by upregulating 24-hydroxylase[49]. However, in
527 the $^{SM22a}CaSR^{\Delta flox/\Delta flox}$ mice, PTH and 1,25-D_3 levels were increased in KO mice despite the
528 elevated FGF23 levels, indicating resistance of PTH and 1,25-D_3 synthesis to control by FGF23
529 and pointing away from FGF23 as sole primary factor. It is possible though that the high 1,25-
530 D_3 and FGF23 levels actually mitigate PTH secretion, contributing to the only relatively mild
531 increase in serum PTH in these mice – although there seems to be a degree of resistance to 1,25-
532 D_3 and serum Ca^{2+} there as well. Taken together, given its resistance to control by FGF23, 1,25-
533 D_3 could be the integrating element leading to the combined and complex phenotype observed
534 in these mice.

535 However, FGF23 resistance does not seem to be a *general* feature of the $^{SM22a}CaSR^{\Delta flox/\Delta flox}$
536 mice, as regulation of renal phosphate reabsorption is apparently not affected. A factor that
537 might play a role here is α-Klotho, which is acting both locally as co-factor for FGF23 and
538 systemically in hormonal fashion[51]. Indeed, the observed hypercalcemia, elevated 1,25-D_3 and
539 FGF23 levels and osteopenia of the $^{SM22a}CaSR^{\Delta flox/\Delta flox}$ mice are, except for the elevated PTH
540 levels, somewhat reminiscent of the phenotype of the global Klotho$^{-/-}$ mice (**Table 4**). This
541 suggests a common role for the VSMC-CaSR and α-Klotho in Ca^{2+} and Pi homeostasis, as
542 already suggested by the biochemical interaction between CaSR and α-Klotho in the PTG[52] and
543 in the kidney[53]. The kidney is the major site of α-Klotho production[54] where changes in serum
544 and urinary α-Klotho mirror those of renal α-Klotho levels[55]. Interestingly, in the
545 $^{SM22a}CaSR^{\Delta flox/\Delta flox}$ mice, even though renal α-Klotho levels were increased, vascular or
546 circulating α-Klotho levels were not affected, suggesting that absence of CaSR from VSMC
547 influences circulating and local α-Klotho metabolism differently.
548 Elevated serum FGF23 may be an independent predictor of cardiovascular mortality[56].
549 Experimentally, FGF23 alone can directly induce LVH[57] and FGF23 gain of function leads to
550 volume expansion, hypertension, and cardiac hypertrophy[58]. Despite chronically elevated
551 FGF23 levels, our $^{SM22a}CaSR^{\Delta flox/\Delta flox}$ mice did not develop LVH at 14 months of age and we
552 did not observe increased mortality[17, 37]. Since these mice are hypotensive despite their
553 chronically elevated FGF23 levels, vascular contractility may play a larger role here than
554 FGF23 mediated renal and cardiac effects on blood pressure.

555 ***Renal phenotype***

556 The expression of TRPV5, calbindin D28K and PMCA were all increased in the kidneys of the
557 $^{SM22a}CaSR^{\Delta flox/\Delta flox}$ mice, suggesting higher transcellular Ca^{2+} reabsorption. This increase, due
558 to chronic elevation of 1,25-D_3, PTH, and FGF23[58] levels, may contribute to their
559 hypercalcemia, whereas the increased renal NCC expression is likely to contribute to the

560 observed hypercalciuria, as serum and urine Mg^{2+} levels were unaffected in KO mice,
561 suggesting that the abnormality indeed lies within the NCC-expressing distal convoluted
562 tubule[59], rather than the thick ascending limb, where Ca^{2+} and Mg^{2+} reabsorption happen in
563 parallel driven by the transepithelial potential difference[60].

564 The hypercalciuria and hyperphosphaturia of the $^{SM22a}CaSR^{\Delta flox/\Delta flox}$ mice could be the cause for
565 the formation of the observed micro crystals in their urine. We did not observe nephrolithiasis
566 in these animals, which can be explained by a CaSR-mediated compensatory mechanism of
567 urine dilution and acidification. In the collecting duct principal cells, the CaSR[61] is co-expressed
568 luminally with AQP2[39, 62-65], and decreases water reabsorption by reducing the apical insertion
569 of AQP2 water channels. In intercalated cells, the CaSR induces luminal acidification by
570 activating the V-type H^{+} ATPase. In $^{SM22a}CaSR^{\Delta flox/\Delta flox}$ mice, renal AQP2 expression levels
571 were reduced while urinary excretion of degraded AQP2 was increased, indicating decreased
572 water reabsorption, and explaining the reduction of urine osmolality. Furthermore, renal V-
573 ATPase expression was increased in $^{SM22a}CaSR^{\Delta flox/\Delta flox}$ mice compared to WT controls,
574 explaining their acidified urine.

575 Implications and conclusions

576 Our study may also have important clinical implications. Physiological pulsation is necessary
577 for the maintenance of CaSR expression in human aortic smooth muscle cells and may protect
578 arteries from developing VC[66]. Thus, in early CKD, an increase in arterial stiffness and blood
579 pressure, could potentially yield a reduction in CaSR expression by VSMC. While absence of
580 the CaSR apparently does not prompt immediate VC in the blood vessels *in vivo*, it could
581 contribute to the disease onset *via* the deleterious effects of VSMC-CaSR loss on mineral ion
582 homeostasis, as observed in our mouse model. A reduction in blood pressure could thus slow
583 the VSMC-CaSR loss-induced disease progression. Furthermore, a reduction in blood pressure
584 below what is recommended by most guidelines led to improved cardiovascular and all-cause

585 mortality in the CKD population[67]. Our study supports these findings and points to an early
586 targeting of blood pressure control to delay CKD progression. Owing to their ability to affect
587 the VSMC-CaSR, calcimimetics would also be expected to be directly vasculoprotective, in
588 addition to their systemic effects mediated by suppression of circulating PTH and FGF23 levels.
589
590 The VSMC-CaSR apparently contributes to mineral ion homeostasis control, possibly by direct
591 control of FGF23 and 1,25-D_3 production / secretion, though the phenotype of the
592 $^{SM22a}CaSR^{\Delta flox/\Delta flox}$ mouse is likely to be the result of a combination of disturbances acting
593 together. Global deletion of the CaSR from VSMC might affect calcium-sensing in all
594 calciotropic organs to some degree, suggesting a role for the VSMC-CaSR in contributing to
595 each individual organ's response to mineral ion homeostasis. Further work will be necessary to
596 dissect the organ-specific paracrine/autocrine responses *vs* whole body endocrine feedback
597 mechanisms for the fine control of mineral ion homeostasis that the VSMC-CaSR evidently
598 supports.
599

Author contributions

DR, WC, and MSch designed the study;
MSch, MR, ILF, TSW, SCB, PLY, JG, TM, MSa, CLT, CM, HQ, SAP, DTW, TG, VVM, RAF, AH, JH, CSM and WC carried out experiments;
MSch, MR, TSW, CM, RAF, UKH, DTW, VVM, TG, CSM, JH, WC, EK and GV analyzed the data;
MSch, MR, TSW and WC made the figures;
MSch, MR, WC, SCB, GV, SAP, VVM, RAF, EK and DR drafted and revised the paper;
All authors approved the final version of the manuscript.

Acknowledgements

The authors want to acknowledge B. Monk, B. van der Kolk, A. Wheatley, P. Edwards, and N. Kupper for their help with some of the initial experiments and revisions, and Professor AE Canfield and Dr B. Richards for helpful discussions.

Disclosures

The authors have no disclosures and no competing financial interests.

Funding

EU Marie Curie Innovative Training Network Grant FP7-264663 “Multifaceted CaSR” (to DR, SAP and EK), Austrian Science Fund P-29948-B28 (to EK), Austrian Science Fund and Herzfelder’sche Familienstiftung P-32840-B (to MSch), “Intervento cofinanziato dal Fondo di Sviluppo e Coesione 2007-2013–APQ Ricerca Regione Puglia, Programma Regionale a Sostegno della Specializzazione Intelligente e della Sostenibilità Sociale ed Ambientale – FutureInResearch.” CHVNKZ4 (to MR), Kidney Research UK (Intercalated Scholarship) (to UKH), NIH R01DK12165601, R01DK122259, and VA-BLR&D I01BX005851 and 1IK6BX004835 (to WC).

625 ## References

626 1. London GM, Marchais SJ, Guerin AP, Metivier F: Arteriosclerosis, vascular calcifications
627 and cardiovascular disease in uremia. *Curr Opin Nephrol Hypertens,* 14**:** 525-531, 2005
628 2. Villa-Bellosta R, Millan A, Sorribas V: Role of calcium-phosphate deposition in vascular
629 smooth muscle cell calcification. *Am J Physiol Cell Physiol,* 300**:** C210-220, 2011
630 10.1152/ajpcell.00229.2010
631 3. Yamada S, Giachelli CM: Vascular calcification in CKD-MBD: Roles for phosphate, FGF23,
632 and Klotho. *Bone,* 100**:** 87-93, 2017 10.1016/j.bone.2016.11.012
633 4. Block GA, Klassen PS, Lazarus JM, Ofsthun N, Lowrie EG, Chertow GM: Mineral
634 metabolism, mortality, and morbidity in maintenance hemodialysis. *J Am Soc Nephrol,*
635 15**:** 2208-2218, 2004 10.1097/01.ASN.0000133041.27682.A2
636 5. Riccardi D, Valenti G: Localization and function of the renal calcium-sensing receptor. *Nat*
637 *Rev Nephrol,* 12**:** 414-425, 2016 10.1038/nrneph.2016.59
638 6. Yu L, Tomlinson JE, Alexander ST, Hensley K, Han CY, Dwyer D, et al.: Etelcalcetide, A
639 Novel Calcimimetic, Prevents Vascular Calcification in A Rat Model of Renal
640 Insufficiency with Secondary Hyperparathyroidism. *Calcif Tissue Int,* 101**:** 641-653,
641 2017 10.1007/s00223-017-0319-7
642 7. Moe SM, Seifert MF, Chen NX, Sinders RM, Chen X, Duan D, et al.: R-568 reduces ectopic
643 calcification in a rat model of chronic kidney disease-mineral bone disorder (CKD-
644 MBD). *Nephrol Dial Transplant,* 24**:** 2371-2377, 2009 10.1093/ndt/gfp078
645 8. Parfrey PS, Drueke TB, Block GA, Correa-Rotter R, Floege J, Herzog CA, et al.: The Effects
646 of Cinacalcet in Older and Younger Patients on Hemodialysis: The Evaluation of
647 Cinacalcet HCl Therapy to Lower Cardiovascular Events (EVOLVE) Trial. *Clin J Am*
648 *Soc Nephrol,* 10**:** 791-799, 2015 10.2215/CJN.07730814
649 9. Alam MU, Kirton JP, Wilkinson FL, Towers E, Sinha S, Rouhi M, et al.: Calcification is
650 associated with loss of functional calcium-sensing receptor in vascular smooth muscle
651 cells. *Cardiovasc Res,* 81**:** 260-268, 2009 10.1093/cvr/cvn279
652 10. Henaut L, Boudot C, Massy ZA, Lopez-Fernandez I, Dupont S, Mary A, et al.:
653 Calcimimetics increase CaSR expression and reduce mineralization in vascular smooth
654 muscle cells: mechanisms of action. *Cardiovasc Res,* 101**:** 256-265, 2014
655 10.1093/cvr/cvt249
656 11. Ciceri P, Elli F, Brenna I, Volpi E, Brancaccio D, Cozzolino M: The Calcimimetic Calindol
657 Prevents High Phosphate-Induced Vascular Calcification by Upregulating Matrix GLA
658 Protein. *Nephron Exp Nephrol,* 122**:** 75-82, 2013 10.1159/000349935
659 12. Ciceri P, Volpi E, Brenna I, Elli F, Borghi E, Brancaccio D, et al.: The combination of
660 lanthanum chloride and the calcimimetic calindol delays the progression of vascular
661 smooth muscle cells calcification. *Biochem Biophys Res Commun,* 418**:** 770-773, 2012
662 10.1016/j.bbrc.2012.01.097
663 13. Koleganova N, Piecha G, Ritz E, Schmitt CP, Gross ML: A calcimimetic (R-568), but not
664 calcitriol, prevents vascular remodeling in uremia. *Kidney Int,* 75**:** 60-71, 2009
665 10.1038/ki.2008.490
666 14. Mendoza FJ, Martinez-Moreno J, Almaden Y, Rodriguez-Ortiz ME, Lopez I, Estepa JC, et
667 al.: Effect of calcium and the calcimimetic AMG 641 on matrix-Gla protein in vascular
668 smooth muscle cells. *Calcif Tissue Int,* 88**:** 169-178, 2011 10.1007/s00223-010-9442-4
669 15. Molostvov G, James S, Fletcher S, Bennett J, Lehnert H, Bland R, et al.: Extracellular
670 calcium-sensing receptor is functionally expressed in human artery. *Am J Physiol Renal*
671 *Physiol,* 293**:** F946-955, 2007 10.1152/ajprenal.00474.2006
672 16. Babinsky VN, Hannan FM, Youhanna SC, Marechal C, Jadoul M, Devuyst O, et al.:
673 Association studies of calcium-sensing receptor (CaSR) polymorphisms with serum

674 concentrations of glucose and phosphate, and vascular calcification in renal transplant
675 recipients. *PloS one,* 10**:** e0119459, 2015 10.1371/journal.pone.0119459
676 17. Schepelmann M, Yarova PL, Lopez-Fernandez I, Davies TS, Brennan SC, Edwards PJ, et
677 al.: The vascular Ca2+-sensing receptor regulates blood vessel tone and blood pressure.
678 *Am J Physiol Cell Physiol,* 310**:** C193-204, 2016 10.1152/ajpcell.00248.2015
679 18. Chang W, Tu C, Chen TH, Bikle D, Shoback D: The extracellular calcium-sensing receptor
680 (CaSR) is a critical modulator of skeletal development. *Sci Signal,* 1**:** ra1, 2008
681 10.1126/scisignal.1159945
682 19. Holtwick R, Gotthardt M, Skryabin B, Steinmetz M, Potthast R, Zetsche B, et al.: Smooth
683 muscle-selective deletion of guanylyl cyclase-A prevents the acute but not chronic
684 effects of ANP on blood pressure. *Proc Natl Acad Sci U S A,* 99**:** 7142-7147, 2002
685 10.1073/pnas.102650499
686 20. Yarova PL, Stewart AL, Sathish V, Britt RD, Jr., Thompson MA, AP PL, et al.: Calcium-
687 sensing receptor antagonists abrogate airway hyperresponsiveness and inflammation in
688 allergic asthma. *Science translational medicine,* 7**:** 284ra260, 2015
689 10.1126/scitranslmed.aaa0282
690 21. Sage AP, Lu J, Tintut Y, Demer LL: Hyperphosphatemia-induced nanocrystals upregulate
691 the expression of bone morphogenetic protein-2 and osteopontin genes in mouse smooth
692 muscle cells in vitro. *Kidney Int,* 79**:** 414-422, 2011 10.1038/ki.2010.390
693 22. Schneider CA, Rasband WS, Eliceiri KW: NIH Image to ImageJ: 25 years of image
694 analysis. *Nat Methods,* 9**:** 671-675, 2012
695 23. Schindelin J, Arganda-Carreras I, Frise E, Kaynig V, Longair M, Pietzsch T, et al.: Fiji: an
696 open-source platform for biological-image analysis. *Nat Methods,* 9**:** 676-682, 2012
697 10.1038/nmeth.2019
698 24. Sun Y, Yu H, Zheng D, Cao Q, Wang Y, Harris D, et al.: Sudan black B reduces
699 autofluorescence in murine renal tissue. *Arch Pathol Lab Med,* 135**:** 1335-1342, 2011
700 10.5858/arpa.2010-0549-OA
701 25. Puchtler H, Meloan SN, Terry MS: On the history and mechanism of alizarin and alizarin
702 red S stains for calcium. *J Histochem Cytochem,* 17**:** 110-124, 1969
703 26. Jono S, Nishizawa Y, Shioi A, Morii H: Parathyroid hormone-related peptide as a local
704 regulator of vascular calcification. Its inhibitory action on in vitro calcification by
705 bovine vascular smooth muscle cells. *Arterioscler Thromb Vasc Biol,* 17**:** 1135-1142,
706 1997
707 27. Moorehead WR, Biggs HG: 2-Amino-2-methyl-1-propanol as the alkalizing agent in an
708 improved continuous-flow cresolphthalein complexone procedure for calcium in serum.
709 *Clin Chem,* 20**:** 1458-1460, 1974
710 28. Leroux-Berger M, Queguiner I, Maciel TT, Ho A, Relaix F, Kempf H: Pathologic
711 calcification of adult vascular smooth muscle cells differs on their crest or mesodermal
712 embryonic origin. *J Bone Miner Res,* 26**:** 1543-1553, 2011 10.1002/jbmr.382
713 29. Cheng Z, Liang N, Chen TH, Li A, Santa Maria C, You M, et al.: Sex and age modify
714 biochemical and skeletal manifestations of chronic hyperparathyroidism by altering
715 target organ responses to Ca2+ and parathyroid hormone in mice. *J Bone Miner Res,*
716 28**:** 1087-1100, 2013 10.1002/jbmr.1846
717 30. Ranieri M, Tamma G, Di Mise A, Russo A, Centrone M, Svelto M, et al.: Negative feedback
718 from CaSR signaling to aquaporin-2 sensitizes vasopressin to extracellular Ca2. *Journal
719 of cell science,* 128**:** 2350-2360, 2015 10.1242/jcs.168096
720 31. Graca JA, Schepelmann M, Brennan SC, Reens J, Chang W, Yan P, et al.: Comparative
721 expression of the extracellular calcium-sensing receptor in the mouse, rat, and human
722 kidney. *Am J Physiol Renal Physiol,* 310**:** F518-533, 2016 10.1152/ajprenal.00208.2015
723 32. Tamma G, Lasorsa D, Ranieri M, Mastrofrancesco L, Valenti G, Svelto M: Integrin
724 signaling modulates AQP2 trafficking via Arg-Gly-Asp (RGD) motif. *Cellular*

725 *physiology and biochemistry : international journal of experimental cellular*
726 *physiology, biochemistry, and pharmaco,* 27**:** 739-748, 2011 10.1159/000330082
727 33. Trimpert C, van den Berg DT, Fenton RA, Klussmann E, Deen PM: Vasopressin increases
728 S261 phosphorylation in AQP2-P262L, a mutant in recessive nephrogenic diabetes
729 insipidus. *Nephrology, dialysis, transplantation : official publication of the European*
730 *Dialysis and Transplant Associatio,* 27**:** 4389-4397, 2012 10.1093/ndt/gfs292
731 34. Sadler AM, Bailey SJ: Validation of a refined technique for taking repeated blood samples
732 from juvenile and adult mice. *Lab Anim,* 47**:** 316-319, 2013
733 10.1177/0023677213494366
734 35. Procino G, Mastrofrancesco L, Tamma G, Lasorsa DR, Ranieri M, Stringini G, et al.:
735 Calcium-sensing receptor and aquaporin 2 interplay in hypercalciuria-associated renal
736 concentrating defect in humans. An in vivo and in vitro study. *PloS one,* 7**:** e33145,
737 2012 10.1371/journal.pone.0033145
738 36. Tamma G, Di Mise A, Ranieri M, Svelto M, Pisot R, Bilancio G, et al.: A decrease in
739 aquaporin 2 excretion is associated with bed rest induced high calciuria. *J Transl Med,*
740 12**:** 133, 2014 10.1186/1479-5876-12-133
741 37. Yarova PL, Stewart AL, Sathish V, Britt RD, Jr., Thompson MA, AP PL, et al.: Calcium-
742 sensing receptor antagonists abrogate airway hyperresponsiveness and inflammation in
743 allergic asthma. *Sci Transl Med,* 7**:** 284ra260, 2015 10.1126/scitranslmed.aaa0282
744 38. Alexander RT, Woudenberg-Vrenken TE, Buurman J, Dijkman H, van der Eerden BC, van
745 Leeuwen JP, et al.: Klotho prevents renal calcium loss. *J Am Soc Nephrol,* 20**:** 2371-
746 2379, 2009 10.1681/ASN.2008121273
747 39. Ranieri M, Zahedi K, Tamma G, Centrone M, Di Mise A, Soleimani M, et al.: CaSR
748 signaling down-regulates AQP2 expression via a novel microRNA pathway in pendrin
749 and NaCl cotransporter knockout mice. *FASEB J,* 32**:** 2148-2159, 2018
750 10.1096/fj.201700412RR
751 40. London GM, Guerin AP, Marchais SJ, Metivier F, Pannier B, Adda H: Arterial media
752 calcification in end-stage renal disease: impact on all-cause and cardiovascular
753 mortality. *Nephrol Dial Transplant,* 18**:** 1731-1740, 2003 10.1093/ndt/gfg414
754 41. Raggi P, Boulay A, Chasan-Taber S, Amin N, Dillon M, Burke SK, et al.: Cardiac
755 calcification in adult hemodialysis patients. A link between end-stage renal disease and
756 cardiovascular disease? *J Am Coll Cardiol,* 39**:** 695-701, 2002 10.1016/s0735-
757 1097(01)01781-8
758 42. Torremade N, Bozic M, Panizo S, Barrio-Vazquez S, Fernandez-Martin JL, Encinas M, et
759 al.: Vascular Calcification Induced by Chronic Kidney Disease Is Mediated by an
760 Increase of 1alpha-Hydroxylase Expression in Vascular Smooth Muscle Cells. *J Bone*
761 *Miner Res,* 31**:** 1865-1876, 2016 10.1002/jbmr.2852
762 43. Adeney KL, Siscovick DS, Ix JH, Seliger SL, Shlipak MG, Jenny NS, et al.: Association of
763 serum phosphate with vascular and valvular calcification in moderate CKD. *J Am Soc*
764 *Nephrol,* 20**:** 381-387, 2009 10.1681/ASN.2008040349
765 44. Ho C, Conner DA, Pollak MR, Ladd DJ, Kifor O, Warren HB, et al.: A mouse model of
766 human familial hypocalciuric hypercalcemia and neonatal severe hyperparathyroidism.
767 *Nat Genet,* 11**:** 389-394, 1995 10.1038/ng1295-389
768 45. Chang W, Tu CL, Jean-Alphonse FG, Herberger A, Cheng Z, Hwong J, et al.: PTH
769 hypersecretion triggered by a GABAB1 and Ca(2+)-sensing receptor heterocomplex in
770 hyperparathyroidism. *Nat Metab,* 2**:** 243-255, 2020 10.1038/s42255-020-0175-z
771 46. Toka HR, Al-Romaih K, Koshy JM, DiBartolo S, 3rd, Kos CH, Quinn SJ, et al.: Deficiency
772 of the calcium-sensing receptor in the kidney causes parathyroid hormone-independent
773 hypocalciuria. *J Am Soc Nephrol,* 23**:** 1879-1890, 2012 10.1681/ASN.2012030323

774 47. Centeno PP, Herberger A, Mun HC, Tu C, Nemeth EF, Chang W, et al.: Phosphate acts
775 directly on the calcium-sensing receptor to stimulate parathyroid hormone secretion.
776 *Nat Commun,* 10**:** 4693, 2019 10.1038/s41467-019-12399-9
777 48. Saito H, Maeda A, Ohtomo S, Hirata M, Kusano K, Kato S, et al.: Circulating FGF-23 is
778 regulated by 1alpha,25-dihydroxyvitamin D3 and phosphorus in vivo. *J Biol Chem,*
779 280**:** 2543-2549, 2005 10.1074/jbc.M408903200
780 49. Shimada T, Hasegawa H, Yamazaki Y, Muto T, Hino R, Takeuchi Y, et al.: FGF-23 is a
781 potent regulator of vitamin D metabolism and phosphate homeostasis. *J Bone Miner*
782 *Res,* 19**:** 429-435, 2004 10.1359/JBMR.0301264
783 50. Shimada T, Kakitani M, Yamazaki Y, Hasegawa H, Takeuchi Y, Fujita T, et al.: Targeted
784 ablation of Fgf23 demonstrates an essential physiological role of FGF23 in phosphate
785 and vitamin D metabolism. *J Clin Invest,* 113**:** 561-568, 2004 10.1172/JCI19081
786 51. Dalton GD, Xie J, An SW, Huang CL: New Insights into the Mechanism of Action of
787 Soluble Klotho. *Front Endocrinol (Lausanne),* 8**:** 323, 2017 10.3389/fendo.2017.00323
788 52. Fan Y, Liu W, Bi R, Densmore MJ, Sato T, Mannstadt M, et al.: Interrelated role of Klotho
789 and calcium-sensing receptor in parathyroid hormone synthesis and parathyroid
790 hyperplasia. *Proc Natl Acad Sci U S A,* 115**:** E3749-E3758, 2018
791 10.1073/pnas.1717754115
792 53. Yoon J, Liu Z, Lee E, Liu L, Ferre S, Pastor J, et al.: Physiologic Regulation of Systemic
793 Klotho Levels by Renal CaSR Signaling in Response to CaSR Ligands and pHo. *J Am*
794 *Soc Nephrol*, 2021 10.1681/ASN.2021020276
795 54. Kuro-o M, Matsumura Y, Aizawa H, Kawaguchi H, Suga T, Utsugi T, et al.: Mutation of
796 the mouse klotho gene leads to a syndrome resembling ageing. *Nature,* 390**:** 45-51, 1997
797 10.1038/36285
798 55. Hu MC, Shi M, Zhang J, Quinones H, Griffith C, Kuro-o M, et al.: Klotho deficiency causes
799 vascular calcification in chronic kidney disease. *J Am Soc Nephrol,* 22**:** 124-136, 2011
800 10.1681/ASN.2009121311
801 56. Arnlov J, Carlsson AC, Sundstrom J, Ingelsson E, Larsson A, Lind L, et al.: Serum FGF23
802 and risk of cardiovascular events in relation to mineral metabolism and cardiovascular
803 pathology. *Clin J Am Soc Nephrol,* 8**:** 781-786, 2013 10.2215/CJN.09570912
804 57. Faul C, Amaral AP, Oskouei B, Hu MC, Sloan A, Isakova T, et al.: FGF23 induces left
805 ventricular hypertrophy. *J Clin Invest,* 121**:** 4393-4408, 2011 10.1172/JCI46122
806 58. Andrukhova O, Slavic S, Smorodchenko A, Zeitz U, Shalhoub V, Lanske B, et al.: FGF23
807 regulates renal sodium handling and blood pressure. *EMBO Mol Med,* 6**:** 744-759, 2014
808 10.1002/emmm.201303716
809 59. Subramanya AR, Ellison DH: Distal convoluted tubule. *Clin J Am Soc Nephrol,* 9**:** 2147-
810 2163, 2014 10.2215/CJN.05920613
811 60. de Rouffignac C, Quamme G: Renal magnesium handling and its hormonal control. *Physiol*
812 *Rev,* 74**:** 305-322, 1994 10.1152/physrev.1994.74.2.305
813 61. Renkema KY, Velic A, Dijkman HB, Verkaart S, van der Kemp AW, Nowik M, et al.: The
814 calcium-sensing receptor promotes urinary acidification to prevent nephrolithiasis. *J Am*
815 *Soc Nephrol,* 20**:** 1705-1713, 2009 10.1681/ASN.2008111195
816 62. Ranieri M: Renal Ca(2+) and Water Handling in Response to Calcium Sensing Receptor
817 Signaling: Physiopathological Aspects and Role of CaSR-Regulated microRNAs. *Int J*
818 *Mol Sci,* 20, 2019 10.3390/ijms20215341
819 63. Sands JM, Naruse M, Baum M, Jo I, Hebert SC, Brown EM, et al.: Apical extracellular
820 calcium/polyvalent cation-sensing receptor regulates vasopressin-elicited water
821 permeability in rat kidney inner medullary collecting duct. *J Clin Invest,* 99**:** 1399-1405,
822 1997 10.1172/JCI119299

823 64. Riccardi D, Brown EM: Physiology and pathophysiology of the calcium-sensing receptor
824 in the kidney. *Am J Physiol Renal Physiol,* 298**:** F485-499, 2010
825 10.1152/ajprenal.00608.2009
826 65. Brown EM: Physiology and pathophysiology of the extracellular calcium-sensing receptor.
827 *Am J Med,* 106**:** 238-253, 1999
828 66. Molostvov G, Hiemstra TF, Fletcher S, Bland R, Zehnder D: Arterial Expression of the
829 Calcium-Sensing Receptor Is Maintained by Physiological Pulsation and Protects
830 against Calcification. *PloS one,* 10**:** e0138833, 2015 10.1371/journal.pone.0138833
831 67. Gosmanova EO, Kovesdy CP: Blood Pressure Targets in CKD: Lessons Learned from
832 SPRINT and Previous Observational Studies. *Curr Cardiol Rep,* 18**:** 88, 2016
833 10.1007/s11886-016-0769-y
834 68. Kaludjerovic J, Komaba H, Lanske B: Effects of klotho deletion from bone during chronic
835 kidney disease. *Bone,* 100**:** 50-55, 2017 10.1016/j.bone.2017.02.006
836

837

838 **Supplemental Material Table of Contents**

839

840 Page numbers refer to the *supplemental material_revised.pdf*

Table S1	Pg. 2
Table S2	Pg. 3
Figure S1	Pg. 4
Figure S2	Pg. 5
Figure S3	Pg. 6
Figure S4	Pg. 7
Figure S5	Pg. 8
Figure S6	Pg. 9
Figure S7	Pg. 10
Figure S8	Pg. 11

841

842

843 # Tables

844 **Table 1: Blood biochemistry of 3-month-old WT and KO mice.** 1,25-D_3 = 1,25-dihydroxy

845 vitamin D / calcitriol, BUN = blood urea nitrogen. * $p < 0.05$, ** $p < 0.01$, *** $p < 0.001$, mean

846 ± SD, two-tailed T-test.

Parameter	Unit	WT			N	KO			N	*p*-value	
Na^+	mmol / l	145.35	±	2.77	17	144.15	±	3.84	10	0.3540	
Cl^-	mmol / l	109.18	±	3.34	17	108.45	±	4.82	10	0.6472	
K^+	mmol / l	5.24	±	0.40	3	5.62	±	0.18	3	0.2092	
Ca^{2+}	mmol / l	2.28	±	0.21	28	2.94	±	0.59	21	<0.0001	***
Mg^{2+}	mmol / l	1.06	±	0.12	22	1.15	±	0.22	20	0.0979	
FGF23	pg / ml	145.0	±	36.4	11	384.4	±	204.5	6	0.0015	**
Pi	mmol / l	2.36	±	0.45	17	1.94	±	0.47	16	0.0146	*
Hematocrit	%	40.3	±	7.6	9	38.9	±	8.6	6	0.7407	
PTH	pg / ml	151.7	±	115.5	30	256.6	±	249.8	30	0.0411	*
1,25-D_3	pmol / l	162.1	±	81.3	19	310.8	±	173.4	17	0.0020	**
α-Klotho	pg / ml	555.4	±	164.6	13	564.7	±	389.3	11	0.9379	
Aldosterone	pg / ml	508.1	±	199.0	12	421.8	±	205.2	12	0.3072	
Renin	pg / ml	123.8	±	58.0	12	115.4	±	40.3	12	0.6850	
Fetuin A	µg / ml	201.4	±	40.9	12	193.0	±	40.8	12	0.6175	
PPi	µmol / l	34.1	±	40.8	12	25.0	±	14.2	12	0.4747	
Albumin	mg / ml	29.4	±	1.4	11	27.6	±	1.7	11	0.0179	*
ALP	U / l	81.73	±	11.38	11	100.18	±	22.74	11	0.0297	*
Creatinine	µmol / l	15.4	±	1.6	6	13.0	±	1.3	5	0.0265	*
Urea	mmol / l	10.1	±	1.3	6	10.4	±	0.3	5	0.6474	
BUN	mmol / l	8.4	±	2.4	11	8.7	±	1.8	11	0.7781	
Total Protein	mg / ml	54.4	±	3.0	6	51.2	±	2.6	4	0.1196	

847

848

849 **Table 2: Urine chemistry of 3-month-old WT and KO mice.** Averages of measurements
850 from two consecutive 24 h urine collections. Cr = creatinine, d = 24 h, BW = body weight (g),
851 Na^+, Cl^-, K^+, Ca^{2+}, Mg^{2+}, and Pi are normalised to individual creatinine levels of each mouse.
852 Creatinine, total urinary protein, urea, uric acid, and glucose are normalised to 24 h urine
853 production per bodyweight of each mouse. * $p < 0.05$, *** $p < 0.001$, mean ± SD, two-tailed
854 T-test.

Parameter	Unit	WT			N	KO			N	*p*-value	
Na^+:Cr	mmol / mmol	37.32	±	9.93	6	34.06	±	12.57	6	0.6290	
Cl^-:Cr	mmol / mmol	70.18	±	10.93	6	69.25	±	19.70	6	0.9215	
K^+:Cr	mmol / mmol	50.25	±	9.27	6	58.62	±	8.86	6	0.1410	
Ca^{2+}:Cr	mmol / mmol	0.90	±	0.55	6	6.48	±	4.56	6	0.0140	*
Mg^{2+}:Cr	mmol / mmol	6.40	±	1.81	4	8.05	±	3.19	3	0.4184	
Pi:Cr	mmol / mmol	7.84	±	2.98	6	22.45	±	5.92	6	0.0003	***
Cr	µmol / (d * BW)	0.230	±	0.038	6	0.221	±	0.061	6	0.7548	
Total protein	µg / (d * BW)	197.43	±	112.49	6	176.34	±	104.42	6	0.7435	
Urea	µmol / (d * BW)	80.23	±	21.42	6	80.42	±	19.88	6	0.9876	
Uric acid	µmol / (d * BW)	37.33	±	8.20	6	32.30	±	11.60	6	0.4069	
Glucose	µmol / (d * BW)	0.133	±	0.030	6	0.219	±	0.178	6	0.2694	
24h urine	mg / h / BW	2.50	±	0.56	6	2.98	±	0.60	5	0.1999	

855

856

857

858 **Table 3: Results of µCT analysis of hind-leg bones from 3-month-old WT and KO mice.**

859 Bone parameter abbreviations: Tb = trabecular bone at the distal femur, Ct = cortical bone at

860 the tibio-fibular junction, TV = total volume, BV = bone volume, BV/TV = bone volume

861 fraction, CD = connectivity density, SMI = structure model index, N = trabecular number, Th

862 = thickness, Sp = spacing, BMD = bone mineral density. AU = arbitrary units. Mean ± SD, * p

863 < 0.05, ** $p < 0.01$, two-tailed Student's t-test.

Parameter	Unit	WT	N	KO	N	*p*-value	
Tb.TV	mm³	2.13 ± 0.25	8	1.88 ± 0.15	9	0.0238	*
Tb.BV	mm³	0.33 ± 0,05	8	0.24 ± 0.04	9	0.0014	**
Tb.BV/TV	ratio	0.16 ± 0.02	8	0.13 ± 0.02	9	0.0133	*
Tb.CD	1/mm³	369.62 ± 39.79	8	285.25 ± 49.53	9	0.0016	**
Tb.SMI	AU	2.07 ± 0.28	8	2.37 ± 0.15	9	0.0123	*
Tb.N	1/mm³	5.91 ± 0.42	8	5.08 ± 0.80	9	0.0189	*
Tb.Th	µm	39.09 ± 5.94	8	37.30 ± 4.49	9	0.4915	
Tb.Sp	mm	0.17 ± 0.01	8	0.19 ± 0.02	9	0.0140	*
Tb.BMD	AU	1164.85 ± 8.75	8	1138.54 ± 23.69	9	0.0098	**
Ct.TV	mm³	0.40 ± 0.03	8	0.39 ± 0.04	9	0.3678	
Ct.BV	mm³	0.27 ± 0.02	8	0.25 ± 0.03	9	0.1977	
Ct.BV/TV	ratio	0.66 ± 0.03	8	0.66 ± 0.03	9	0.5431	
Ct.BMD	AU	1433.39 ± 33.25	8	1394.06 ± 16.96	9	0.0069	**
Ct.Th	µm	235.13 ± 15.15	8	226.56 ± 13.38	9	0.2344	

864

865

866

867 **Table 4: Comparison of the Klotho$^{-/-}$, PTG-CaSR$^{-/-}$, Renal-CaSR$^{-/-}$ and VSMC-CaSR$^{-/-}$**

868 **mice.** Arrows: (fold changes compared to control animals) =: no change, 1-2: ↓/↑; 2-3: ↓↓/↑↑;

869 >3: ↓↓↓/↑↑↑, n.d.: not determined

Parameter	Klotho deficient [54, 68]	PTG-CaSR $^{-/-}$ [18]	Renal-CaSR$^{-/-}$ [46]	VSMC-CaSR$^{-/-}$
Plasma Ca^{2+}	↑	↑↑	=	↑
Urinary Ca^{2+}	n.d.	↑↑↑	↓↓↓	↑↑↑
Plasma Pi	↑	n.d.	=	↓
Urinary Pi	↑	n.d.	n.d.	↑↑
Plasma 1,25-D_3	↑↑	n.d.	=	↑↑
Plasma PTH	↓	↑↑↑	=	↑
FGF23	↑↑	n.d.	n.d.	↑↑
Body weight	↓↓	↓↓↓	=	=/↓
BMD	↓	↓↓↓	=	↓

870

871 ## Figure legends

872 **Figure 1: *In vitro* calcification of isolated VSMC. A:** Photograph of 24-well microplates with
873 cultured VSMC from WT (left two plates) and KO mouse aortas (right two plates) incubated
874 for 10 days with a series of Ca^{2+} (numbers: mM Ca^{2+} in the 3 horizontally adjacent wells) /
875 phosphate (Pi) concentrations (top two plates: 2 mM Pi, bottom two plates: 3 mM Pi) in the
876 growth medium. Cells were then fixed and stained with Alizarin Red S. Darker spots indicate
877 calcium deposits. At 2 mM Pi, WT did not show any calcification independent of the Ca^{2+}
878 concentration, while VSMC from KO mice started to show calcification at 1.6 mM Ca^{2+}. At 3
879 mM Pi, WT cells started to calcify at 1.6 mM Ca^{2+} and KO cells at 1.2 mM Ca^{2+}. **B:**
880 Quantification of Ca^{2+} deposition in WT and KO cells at 3 mM Pi and 1.2, 1.8 or 2.5 mM Ca^{2+}
881 using o-cresolphthalein complexone assay, normalised to the amount of protein (BCA assay)
882 and the normocalcemic (1.2 mM Ca^{2+}) control. Friedmann with Dunn post-hoc test. **C:**
883 Quantification of Ca^{2+} deposition in WT and KO cells at 3 mM Pi and 1.2 mM Ca^{2+} in the
884 presence or absence of 10 nM calcimimetic R-568. Median±IQR, Mann-Whitney-U test. * $p <$
885 0.05, ** $p < 0.01$.

886

887 **Figure 2: Aorta mRNA expression levels and quantitative immunohistochemistry. A:**
888 *Klotho*, **B:** *Cyp27b1*, and **C:** *Sm22α* mRNA expression levels relative to calibrator (mean ΔCT
889 WT). **D & E:** quantitative immunohistochemistry analysis of α-Klotho in smooth muscle and
890 endothelial layer of WT and KO aorta sections. Mean grey values (lower = darker). **F:**
891 representative stainings for α-Klotho used for quantification. **G & H:** quantitative
892 immunohistochemistry analysis of CYP27B1 in smooth muscle and endothelial layer of WT
893 and KO aorta sections. Mean grey values (lower = darker). **I:** representative stainings for
894 CYP27B1 used for quantification. Inserts = IgG negative control. Inserts = IgG negative
895 control. Scale bars = 50 µm.

896

897 **Figure 3: Kidney calcium handling and CaSR expression in $^{SM22\alpha}CaSR^{\Delta flox/\Delta flox}$ mice. A-B:**
898 semi-quantitative Western blot analyses of □-Klotho and the sodium phosphate cotransporter,
899 NaPi2a. **C-F:** quantitative immunohistochemistry of the vitamin D receptor (VDR), the calcium
900 channel Transient Receptor Potential cation channel subfamily V member 5 (TRPV5),
901 calbindin (D28K) and the plasma membrane calcium ATPase (PMCA). **G:** CaSR mRNA
902 expression in whole kidney lysate relative to calibrator (mean ΔCT of WT). **H:** quantitative
903 immunofluorescence analysis of CaSR expression in kidney sections. **I:** semi-quantitative
904 Western blot analysis of CaSR protein expression in whole kidney lysates. Mean±SD, * $p <$
905 0.05, ** $p < 0.01$, *** $p < 0.001$, two-tailed Student's t-test.

906

907 **Figure 4: Kidney water transport in $^{SM22\alpha}CaSR^{\Delta flox/\Delta flox}$ mice. A:** Optical microscopy images
908 of crystal precipitates in urines from WT and KO mice (scale bar: 100 µm). **B:** Urine osmolality
909 and **C:** urine pH of WT and KO mice from two consecutive days in metabolic cages. Mean±SD,
910 ** $p < 0.01$, *** $p < 0.001$ for overall genotype effect, two-way ANOVA. **D-H:** semi-
911 quantitative Western blot analyses of the thiazide sensitive sodium-chloride cotransporter
912 (NCC), V-H^+-ATPase, total aquaporin 2 (AQP2), pS261-AQP2, pS256-AQP2 in WT and KO
913 kidney lysates. **I:** AQP2 excretion measured by ELISA assay in urines from WT and KO.
914 Mean±SD, * $p < 0.05$, ** $p < 0.01$, two-tailed Student's t-test.

915

916 **Figure 5**: **Analysis of the parathyroid glands. A**: Micrographs of isolated parathyroid glands
917 from WT and KO mice. Scale bar = 500 µm. **B**: Immunofluorescence images of isolated
918 parathyroid glands from WT and KO mice, showing comparable staining intensity for the
919 CaSR. Scale bar = 50 µm. **C**: Western Blot analysis of CaSR expression in parathyroid glands,
920 showing equal expression of both the monomer (~130 kDa) and the dimer (~250 kDa) of the
921 CaSR. **D**: PTH release assay in response to increases in extracellular Ca^{2+}. Left panel: raw data,

922 right panel: normalised to PTH release at 0.5 mM Ca^{2+} = 100 % for both WT and KO. Vertical
923 lines indicate Ca^{2+} concentration at half maximal PTH response. N = 3, < 1.4 % total variance
924 explained by genotype as determined by repeated measures two-way ANOVA.
925
926 **Figure 6: Phenotype of the $^{SM22\alpha}$CaSR$^{\Delta flox/\Delta flox}$ mice**. Continuous lines = stimulation, broken
927 lines = inhibition. Greyed out lines = loss of action due to VSMC-CaSR deletion.
928 Loss of the CaSR in VSMC affects whole body mineral ion homeostasis leading to the loss
929 (red X signs) of an inhibitory function on the production / secretion of 1,25-D_3, PTH, and
930 FGF23. At the same time, VSMC-CaSR loss apparently also affects or overrides hormonal
931 control: 1,25-D3 synthesis is apparently resistant to control by FGF23, while PTH secretion is
932 (slightly) increased, pointing to some degree of resistance to control by 1,25-D_3, FGF23, and
933 serum calcium (despite a fully functional CaSR in the parathyroid glands). The increased
934 1,25-D_3 and PTH leads to hypercalcemia followed by hypercalciuria. Pi excretion is increased
935 as a result of the increased PTH and FGF23 levels, leading to low serum Pi. Urine osmolality
936 and pH are decreased to prevent nephrolithiasis. The urinary calcium and phosphate wasting
937 then contributes to the observed bone loss in these animals (not shown in the scheme). Owing
938 to the presence of blood vessels in all organs of the body, it remains to be elucidated whether
939 all the observed features of this phenotype are primary to CaSR deletion from the VSMC,
940 secondary compensatory mechanisms, or a combination of both.

Figure 1

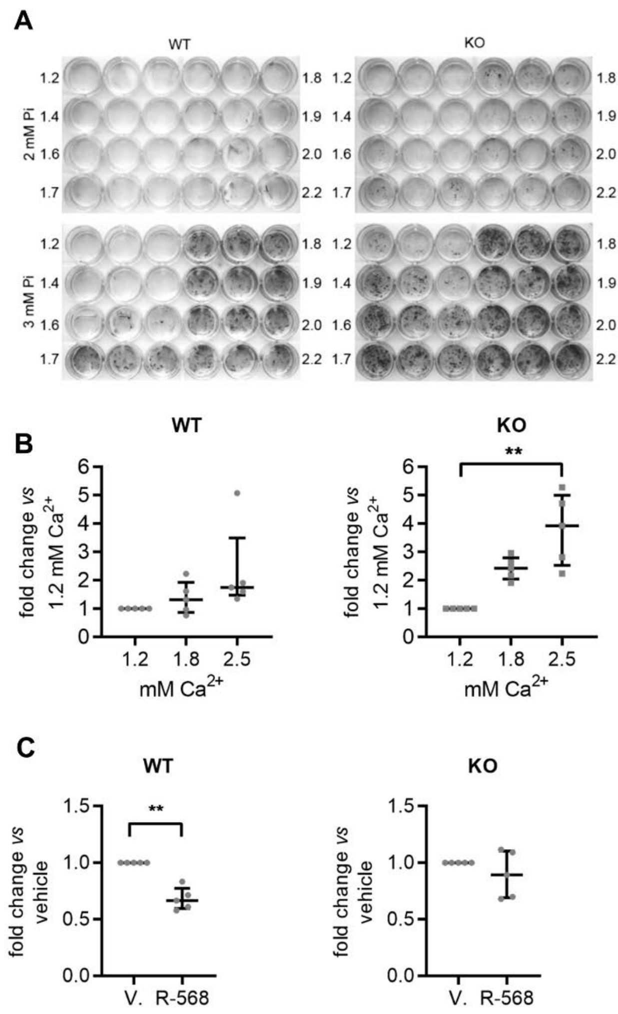

Figure 2

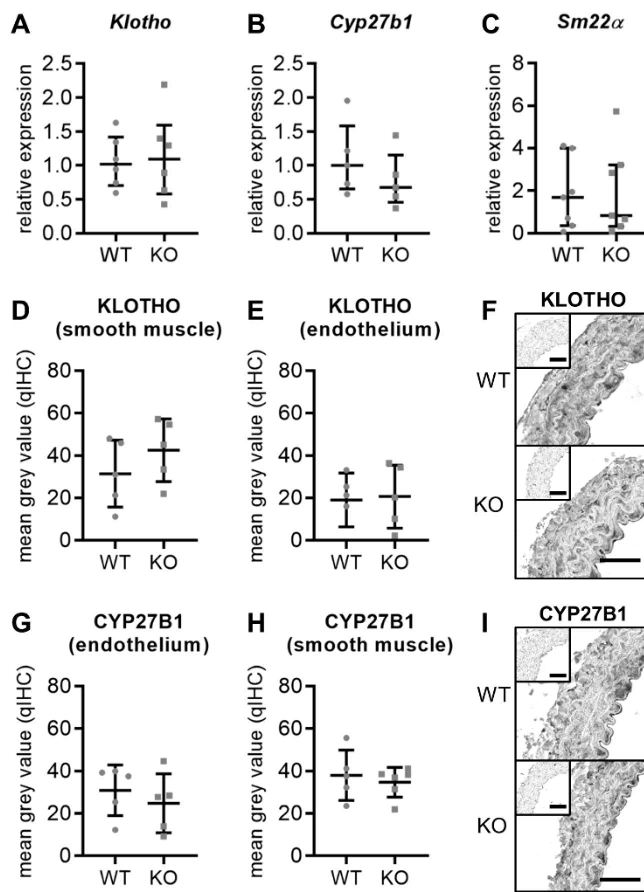

Figure 3

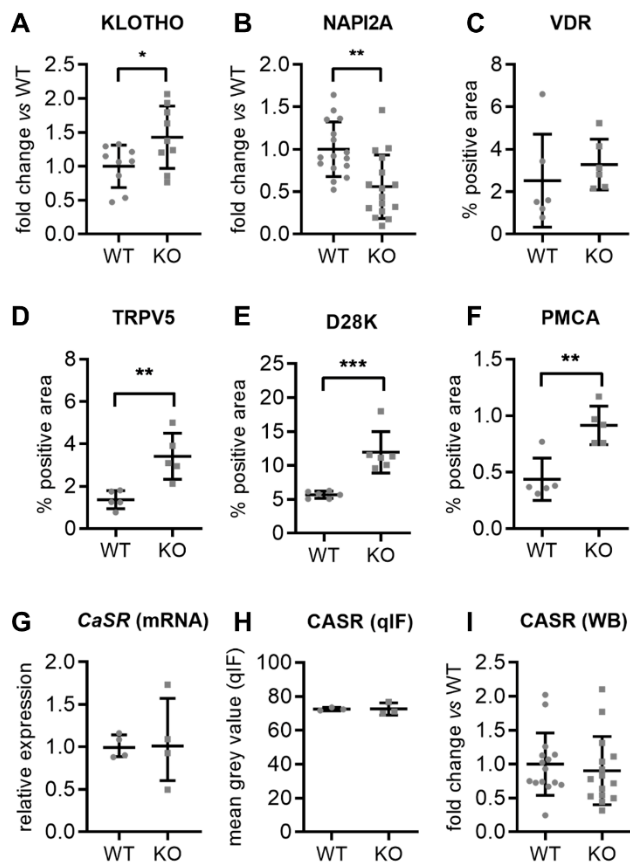

Figure 4

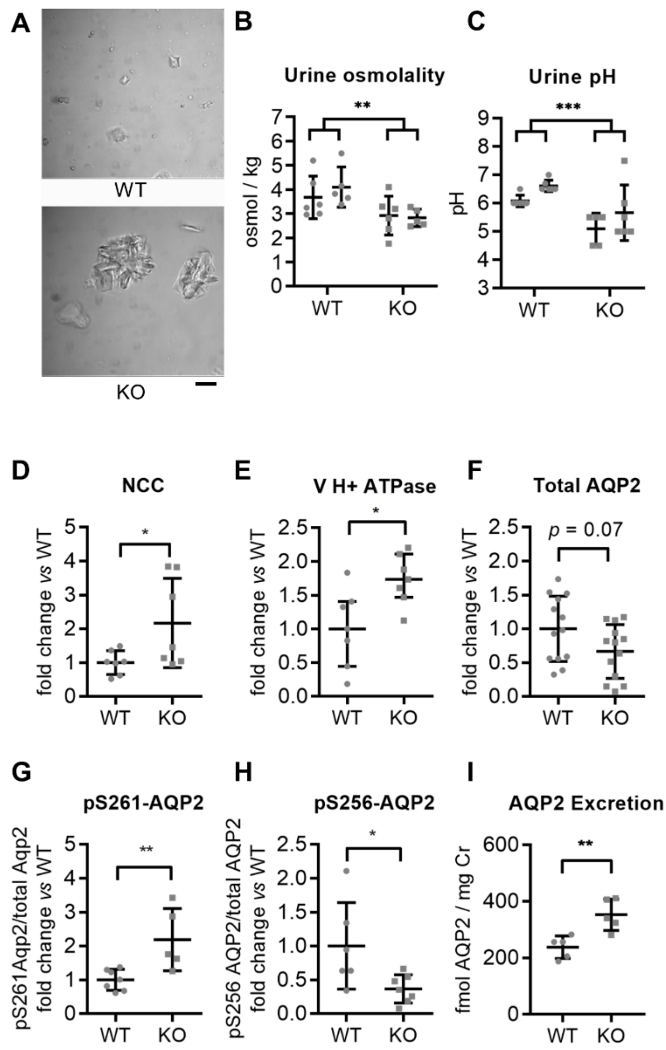

Figure 5

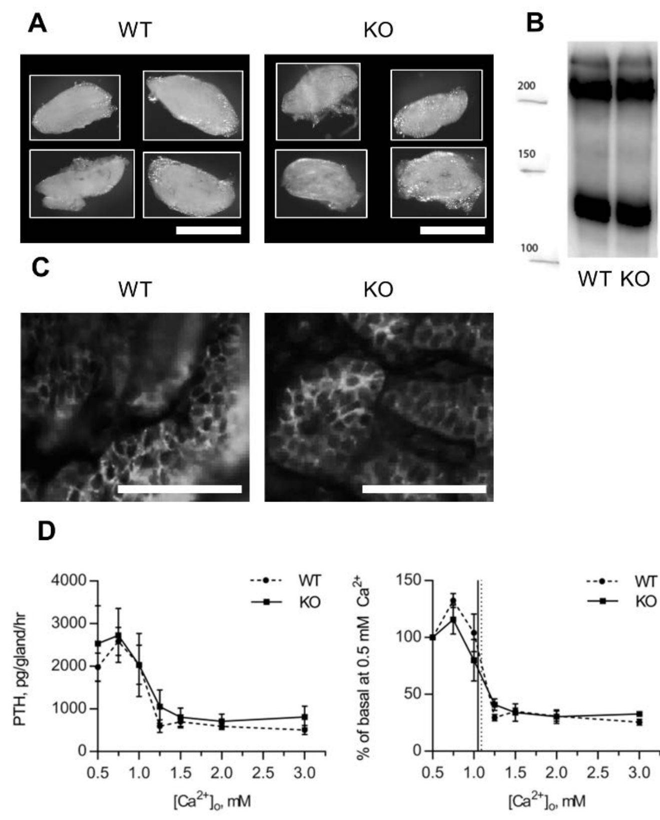

Figure 6

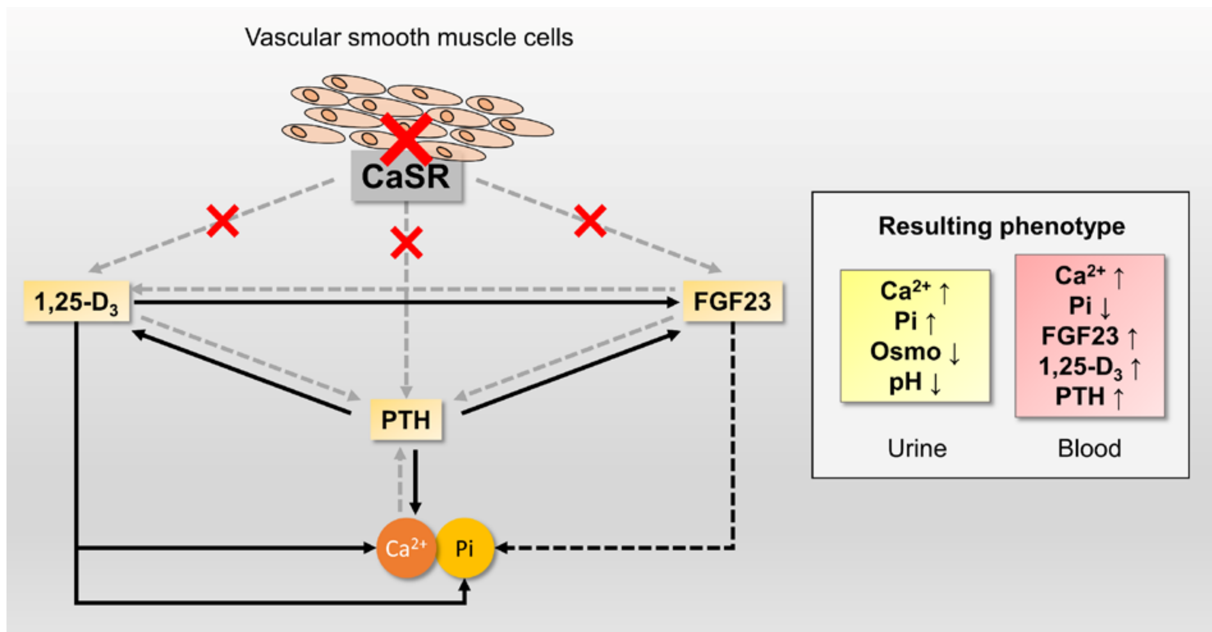

Supplemental material

Table of contents

Table S1	Pg. 2
Table S2	Pg. 3
Figure S1	Pg. 4
Figure S2	Pg. 5
Figure S3	Pg. 6
Figure S4	Pg. 7
Figure S5	Pg. 8
Figure S6	Pg. 9
Figure S7	Pg. 10
Figure S8	Pg. 11

Table S1: Blood biochemistry of 18-month-old WT and KO mouse. * $p < 0.05$, ** $p < 0.01$, mean ± SD, two-tailed T-test. "CaSR" indicates concentration of N-terminal soluble CaSR / CaSR-fragment. Osmolality and CaSR were measured in male and female mice.

Parameter	Unit	WT			N	KO			N	*p*-value	
Na^+	mmol / l	149.0	±	3.61	3	146.3	±	3.06	3	0.3837	
K^+	mmol/l	10.64	±	0.61	3	11.88	±	2.53	3	0.4541	
Cl^-	mmol / l	114.33	±	1.15	3	111.00	±	3.61	3	0.2020	
Ca^{2+}	mmol / l	2.34	±	0.13	3	2.99	±	0.35	3	0.0401	*
Mg^{2+}	mmol / l	1.65	±	0.18	3	2.04	±	0.33	3	0.1369	
FGF23	pg / ml	131.1	±	45.5	3	330.0	±	49.7	3	0.0069	**
α-Klotho	pg / ml	2005.9	±	1342.1	4	1873.0	±	1016.5	4	0.8797	
Osmolality	mosmol/kg	289.2	±	11.7	5	288.1	±	5.6	7	0.8369	
CaSR	ng / ml	2.17	±	0.98	5	2.03	±	0.78	7	0.7816	

Table S2: Organ weights of 6 and 18-month-old animals. WT *vs*. KO, mean ± SD, two-tailed T-test.

Organ	Unit	WT			N	KO			N	*p*-value	
6-month-old animals											
Kidney	mg	235.0	±	32.3	7	232.9	±	23.8	7	0.8899	
Liver	mg	1332.2	±	134.2	8	1445.6	±	190.9	7	0.2016	
Stomach	mg	339.4	±	86.8	8	444.6	±	256.8	7	0.2938	
Spleen	mg	88.1	±	31.3	8	99.1	±	34.3	6	0.5467	
Heart	mg	148.8	±	31.0	8	145.4	±	17.7	6	0.8144	
18-month-old animals											
Kidney	mg	313.1	±	37.6	6	313.0	±	12.9	4	0.9950	
Liver	mg	2294.1	±	461.2	6	2399.8	±	107.9	4	0.6703	
Stomach	mg	846.8	±	372.0	6	738.8	±	247.6	4	0.6268	
Spleen	mg	129.1	±	52.6	6	101.6	±	24.8	4	0.3637	
Heart	mg	201.8	±	20.4	5	231.9	±	8.4	4	0.0285	*

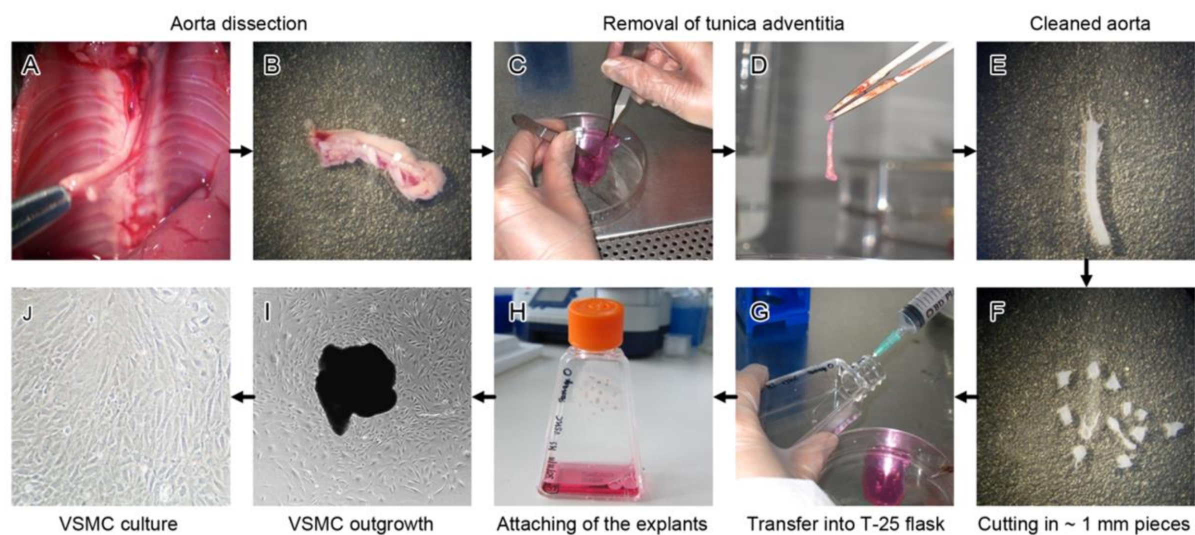

Figure S1: Generation of explant derived aortic VSMC. A: The thoracic aorta is dissected from the spine and **B:** removed to a Petri dish filled with sterile isolation medium where **C and D:** the vessel is cleared from tunica adventitia by gently pulling / scraping the connective tissue until **E:** only the semi-translucent tunica media remains. **F:** The vessel is then cut into small (ca. 1 mm) pieces that are then **G:** transferred into a T-25 cell culture flask by the use of a hypodermic needle. **H:** The flask is kept in an upright position at 37 °C for 10–15 minutes so that the explants are not in contact with medium and can attach firmly to the surface of the flask. 5 ml isolation medium is added, and the explants are kept at 37 °C / 95 % relative humidity (rh) / 5 % CO2 for ca. 7 days after which the medium is changed. **I:** VSMC will start to grow out of the explants. **J:** After ca. 2-3 weeks, the explants are removed and the VSMC passaged to generate a monolayer of cells.

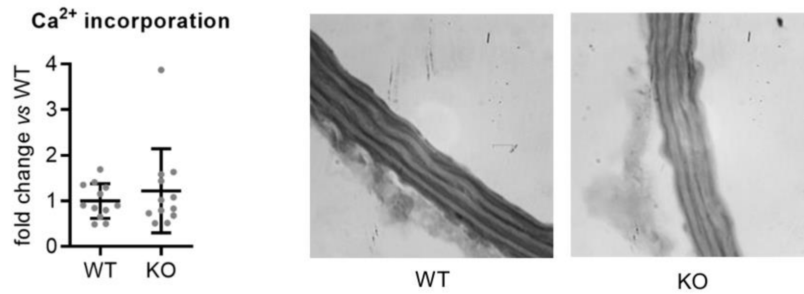

Figure S2: ***Ex vivo* aortic calcification.** Graph: Quantification of Ca^{2+} deposition in WT and KO aortas or 3-month-old mice. Mean±SD. Pictures: Alizarin Red S stainings of thoracic aorta sections from 12-month-old WT and KO animals incubated for 10 days in the presence of medium containing 1.8 mM Ca^{2+} and 3 mM Pi.

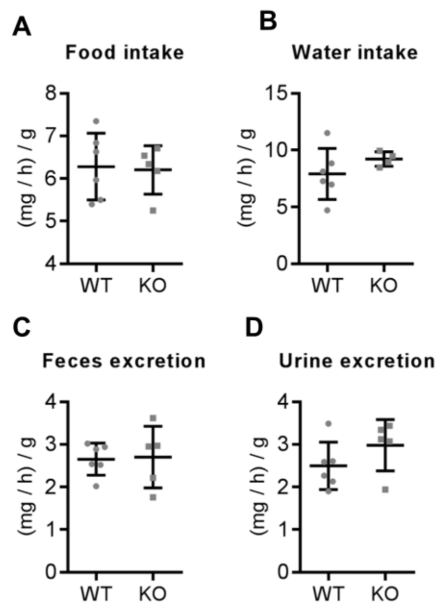

Figure S3: Metabolic cage studies of WT and KO mice. A. Food intake, **B**: Water intake, **C**: Feces excretion, **D**: Urine excretion. Data are shown as consumption (in mg) per h per g bodyweight. Mean±SD.

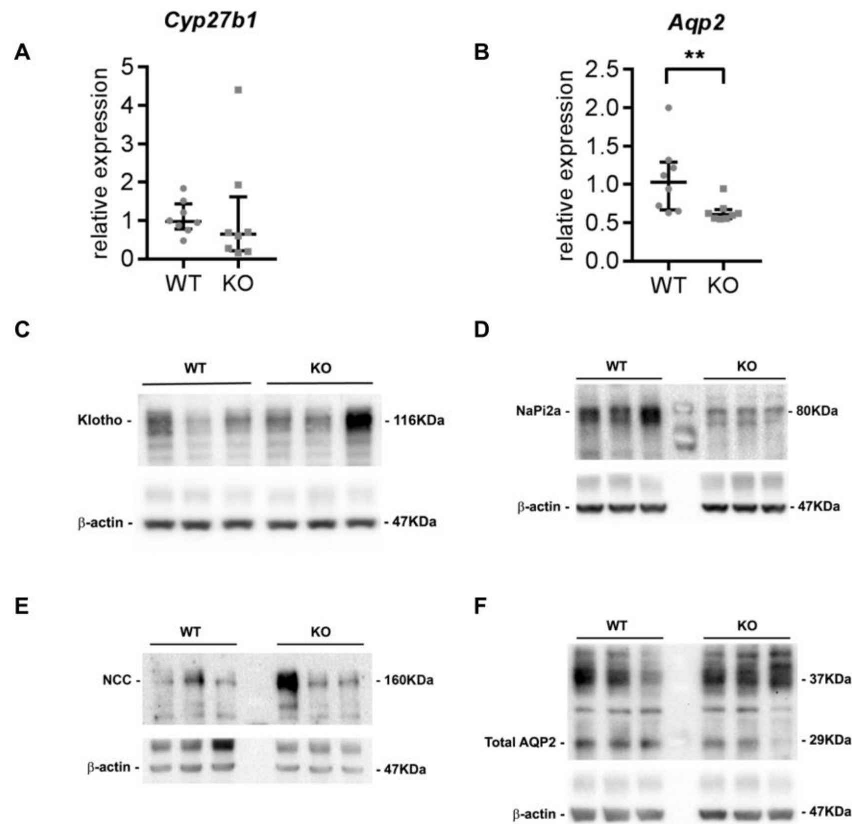

Figure S4: **Supplemental kidney mRNA and protein expression. A:** *Cyp27b1*, and **B:** *Aqp2* mRNA expression levels relative to calibrator (mean ΔCT WT). Representative Western blots showing **C:** Klotho, **D:** NaPi2a, **E:** NCC, **F:** AQP2 expression in kidneys from WT and KO mice.

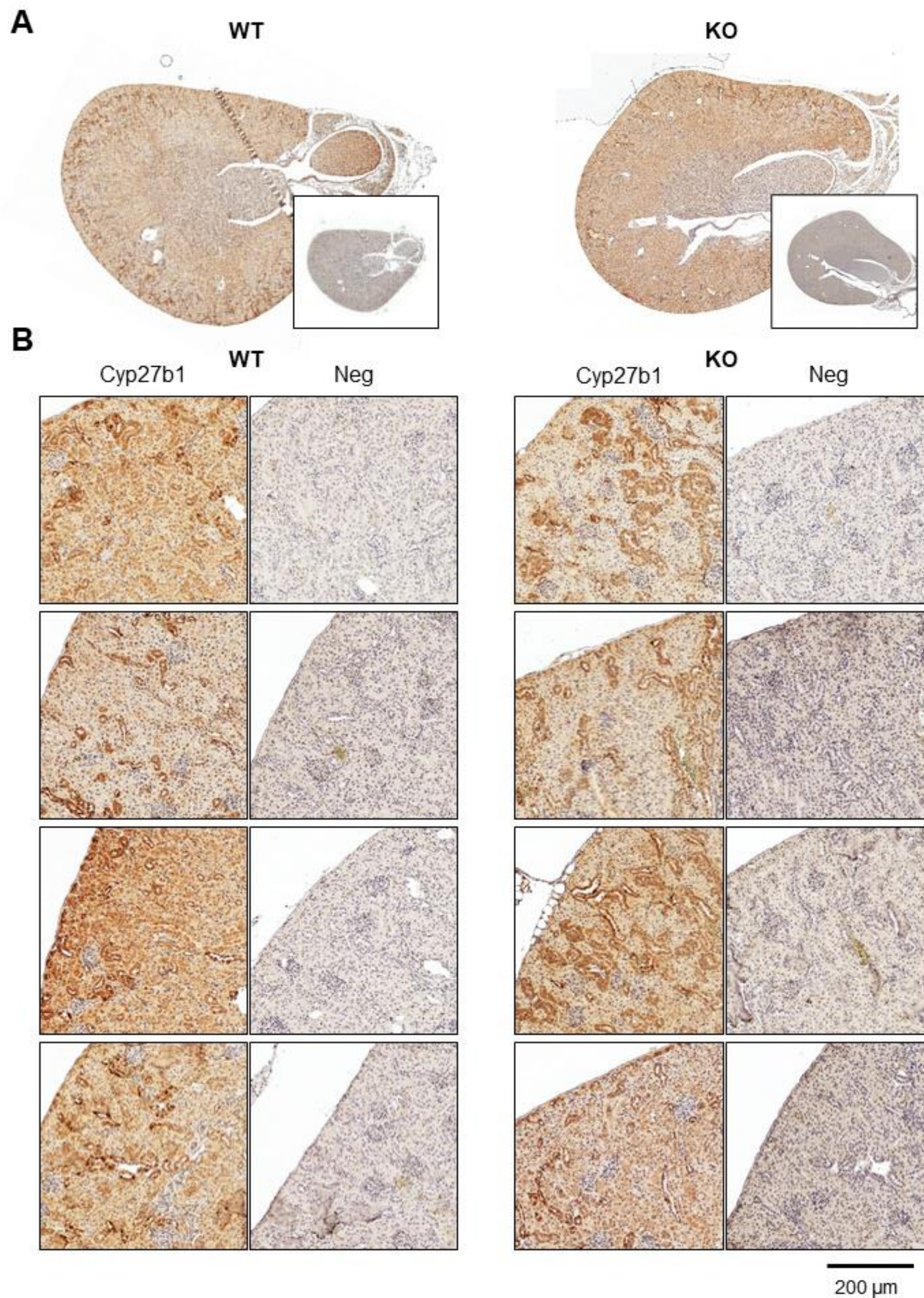

Figure S5: Immunohistochemistry stainings of Cyp27b1 in kidneys of WT and KO mice. Stainings were performed as described in the methods section for Cyp27b1 using the LSBio (Seattle, USA) rabbit anti-Cyp27b1 antibody at 1:1000 dilution. **A:** Overview of representative whole kidney sections stained for Cyp27b1. Insert: negative control. **B:** Cortex of N=4 WT and KO kidneys stained for Cyp27b1 and respective negative controls.

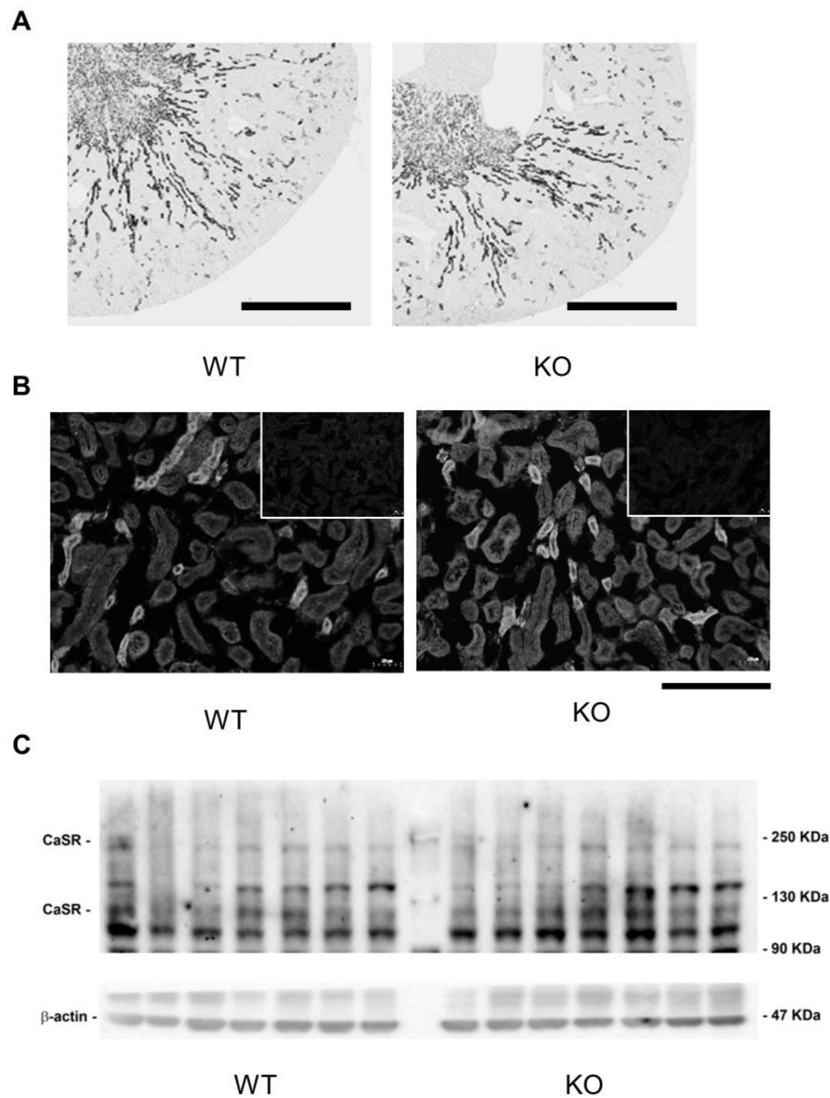

Figure S6: Supplemental kidney CaSR expression data and representative images from Figure 3. A: immunohistochemistry of CaSR expression pattern in WT and KO kidney sections. Scale bar = 1 mm. **B:** immunofluorescence analysis of CaSR expression levels in WT and KO kidneys used for quantitative immunofluorescence analysis. Scale bar = 200 µm. **C:** representative Western blot for CaSR in the kidney (~120-150 kDa: monomer; 250 kDa: dimer).

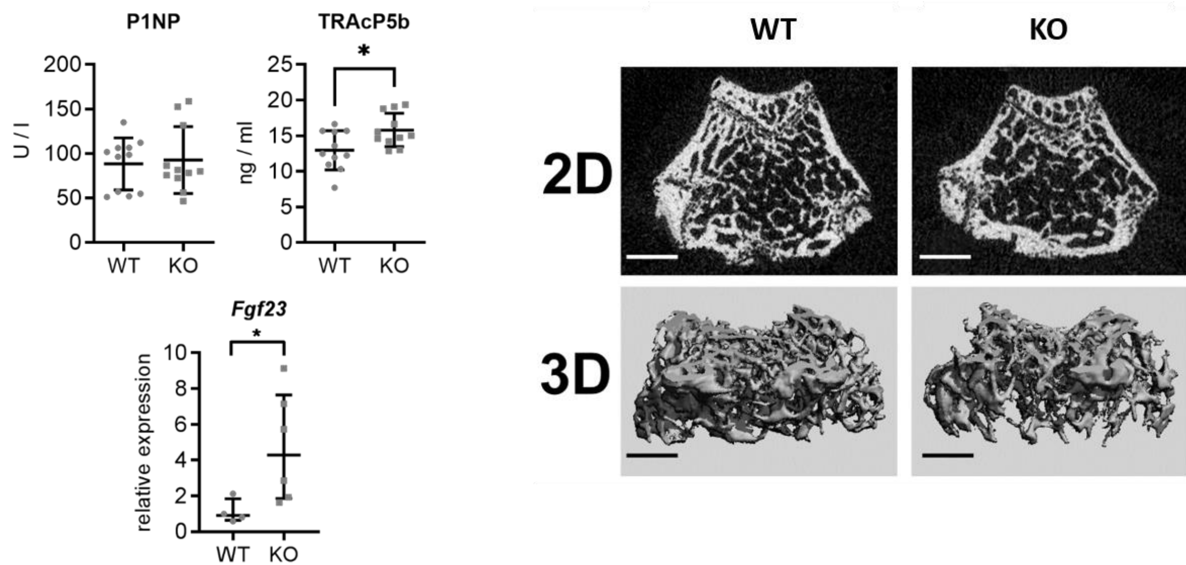

Figure S7: Plasma levels of bone metabolism markers procollagen type 1 (P1NP) and Tartrate-resistant acid phosphatase 5b (TRAcP5b), Fgf23 mRNA expression in bone, and µCT. Bone metabolism markers: * $p < 0.05$, two tailed T-test; measured in male and female mice. RT-qPCR: * $p < 0.05$, Mann-Whitney test. µCT: representative 2-dimension (2D) radiographs and 3-dimension (3D) reconstructed images from distal femurs of 3 months old KO and WT (control) littermates. The 2D radiographs were taken 100 µm below the growth plate. Scale bar: 400 µm

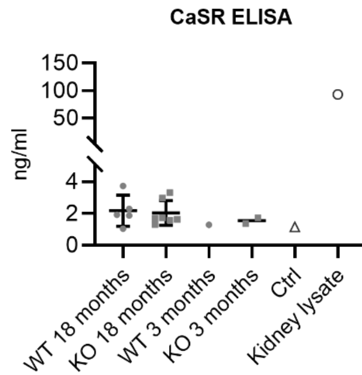

Figure S8: Serum levels of "soluble" CaSR / CaSR fragment. N = 5 (WT, 18 months), N = 7 (KO, 18 months), N = 3 (WT, 3 months), and N = 3 (KO, 3 months). Three of the 3-month samples, (2 WT, 1 KO) were below the detection range and are thus not included in the graph. An additional serum sample of a genetically non-modified 14 month-old mouse ("Ctrl") was added for reference, which had a comparable level of CaSR in the serum. Finally, a sample of 100 mg / ml kidney lysate from a genetically non-modified mouse was tested as positive control.